https://doi.org/10.5194/egusphere-2026-5348
Preprint. Discussion started: 7 September 2026

Quantifying the impact of a projected Record-Breaking 2026–2027 El Niño on Global Temperatures using a Statistical Model

Baptiste Boussemart[1]

[1]Independent researcher, Rouen, France

Correspondence: Baptiste Boussemart (bboussemart.pro@gmail.com)

Abstract. As a potentially record-breaking El Niño for the modern era is forecast for 2026-2027, a key question is how much of the resulting global temperature response to such an unprecedented regime can be attributed to the El Niño-Southern Oscillation (ENSO) relative to the background anthropogenic warming trend over late 2026 and 2027. To explore this question, we introduce TESR, a Ridge regression-based model designed to quantify the influence of ENSO on Global Mean Surface Temperature Anomalies (GMSTA) and to produce probabilistic projections conditioned on ENSO, providing a simple and reproducible way to update these estimates as new seasonal forecasts become available. The model performance was evaluated through out-of-sample walk-forward validation and retrospective probabilistic forecasts. Using Niño 3.4 index as a delayed predictor of the GMSTA response while allowing a non-linear sensitivity that can evolve with the background warming trend, TESR achieves a 47.4 % reduction in retrospective RMSE against a simple ENSO Ordinary Least Squares (OLS) trend benchmark and a Brier Skill Score of 0.798 against per-origin climatology. Initialized with the August C3S multi-model seasonal forecast, TESR projects a GMSTA remaining around +1.9 °C above pre-industrial levels throughout January-May 2027, the period during which the influence of El Niño on global temperatures is simulated as being at its peak, with a median peak of +1.91 °C in March 2027. The model further estimates a 23-24 % likelihood of temporarily exceeding +2.0 °C relative to the pre-industrial period during the 2027 spring season, whereas the +1.5 °C Paris Agreement threshold is highly likely to be surpassed for several months, leading to high chances that 2027 ends up as the warmest year ever recorded since instrumental records began, ranging from +1.57 to +1.92 °C above pre-industrial levels under the August initialized model ENSO trajectory hypothesis. When accounting for the historical underestimation of the strongest temperature peaks by TESR, this probability rises to 45-60 % in sensitivity tests. An ENSO-neutral counterfactual indicates that El Niño substantially increases the probability of crossing both thresholds, though the background warming trend remains the primary driver of the projected anomaly. Since the projected ENSO amplitude used to drive the model for 2026-2027 exceeds the historical range used for model training, we suggest a careful interpretation of the results that should be viewed as experimental rather than a definitive short-term climate forecast.

https://doi.org/10.5194/egusphere-2026-5348
Preprint. Discussion started: 7 September 2026

1 Introduction

One of the main sources of seasonal predictability and interannual climate variability globally is the El Niño-Southern Oscillation (ENSO) (McPhaden et al., 2006). The anomalous warming of the central and eastern equatorial Pacific is the hallmark of El Niño, its warm phase, which usually lasts for several seasons. It usually takes several months for it to have an impact on the Global Mean Surface Temperature Anomaly (GMSTA) (Trenberth et al., 2002), reflecting how tropical and extratropical teleconnections work together. As a result, ENSO is a significant source of short-term global temperature predictability at lead times of several months, with initialized seasonal forecasts maintaining more skill than would be predicted from the long-term warming trend alone.

Quantifying how a given ENSO state translates into a contribution to global temperature is therefore useful for interpreting such forecasts. By simulating interactions between the ocean, atmosphere, land, and cryosphere, dynamic seasonal prediction systems offer a physically comprehensive way to depict this response. However, their computational cost and complexity can make rapid and independently reproducible assessments of a prescribed ENSO scenario challenging. As a complementary option, statistical methods enable the evaluation and updating of empirical ENSO-temperature relationships at a significantly reduced computational cost. Recent research emphasizes the significance of ENSO in seasonal forecast accuracy and indicates that these relationships can capture a significant portion of predictable global mean temperature variability (Tippett and Becker., 2024).

Several methodological challenges nevertheless remain when a statistical ENSO-GMSTA relationship is used prospectively. First, the contemporaneous Niño 3.4 (5°N–5°S, 170°W–120°W) anomaly may not be the most informative predictor of GMSTA due to the delayed and seasonally dependent response of global temperature to ENSO. In addition, the empirical sensitivity of global temperature to ENSO may change with the background state. A further challenge concerns the representation of predictive uncertainty. A simple parametric distribution may not adequately capture the temporal dependence, asymmetry, or non-Gaussianity of forecast errors, while uncertainty in the future ENSO trajectory introduces an additional source of dispersion. These considerations become particularly important when the quantity of interest is the probability of exceeding a temperature threshold instead of the conditional mean.

The developing 2026-2027 El Niño provides a challenging test of these issues. At the time of writing, operational forecasts indicated a rapidly strengthening event, with NOAA's Climate Prediction Center reporting a greater than 90 % probability of a very strong El Niño during boreal autumn and winter 2026–2027. The July 2026 Niño-3.4 anomaly was +1.4 °C, while the October–December 2026 outlook assigned a 69 % probability to a historically strong event exceeding +2.5 °C in the three-month Relative Oceanic Niño Index (RONI), relative to events observed since 1950 (CPC, 2026). Most of the multi-system C3S seasonal forecast systems initialized in August produced peak El Niño amplitudes at least comparable to the strongest events of the previous century and showed continued intensification through late 2026.

https://doi.org/10.5194/egusphere-2026-5348
Preprint. Discussion started: 7 September 2026

Historical strong El Niño events therefore provide an important benchmark for the model before considering such an extrapolation. During the 1982–1983, 1997–1998, and 2015–2016 events, which span a broad range of observed ENSO intensities, the global mean surface temperature showed a noticeable but temporary increase. By taking these events into account, the model-derived ENSO contribution can be evaluated in a number of well-observed cases before being applied to the 2026-2027 scenario. They are therefore not considered direct analogs for the upcoming event, but rather historical validation cases. The comparison examines whether the estimated ENSO contribution varies coherently with the timing and magnitude of the observed ENSO forcing, providing a historical reference for interpreting the model outside its training range.

The prospect of increasingly extreme ENSO events also motivates the development of a framework that can be updated rapidly. Climate-model experiments and observational analyses have suggested that anthropogenic warming can modify the characteristics of ENSO, including the frequency, amplitude or spatial expression of extreme events, although the magnitude and robustness of these changes remain dependent on the model, event definition and metric considered (Cai et al., 2014; Cai et al., 2021; Shin et al., 2022). If the characteristics of ENSO events continue to change, a statistical framework developed for a single event would have limited broader applicability. Instead, a repeatable approach that can be updated whenever new ENSO forecasts are available might offer a helpful supplementary tool for evaluating the effects of future strong events on global temperatures.

In this work, we use the term "ENSO contribution" in a counterfactual, model-based sense. It is defined as the difference, with all other statistical model components held constant, between the GMSTA predicted under a given ENSO scenario and that predicted under an ENSO-neutral counterfactual. This quantity should not be interpreted as a causal physical attribution of the observed global temperature anomaly or as implying that ENSO is solely responsible for observed global warming. Rather, it provides a directly interpretable decomposition of the projected anomaly into an ENSO-dependent component and a background component, and quantifies the conditional contribution of the specified ENSO trajectory within the statistical model.

To quantify this contribution, we introduce TESR (Temperature-ENSO Statistical Regression), a parsimonious statistical framework designed for short-lead global temperature projections. TESR combines a nonlinear background temporal component with a lagged and smoothed Niño 3.4 predictor, an interaction between ENSO and time allowing the empirical ENSO sensitivity to evolve, a residual seasonal component and Ridge regularization. Instead of being imposed through a Gaussian error assumption, predictive uncertainty is empirically estimated from out-of-sample residuals using block bootstrap resampling. Walk-forward validation is used to assess retrospective predictive performance, including comparison with a simple trend-ENSO benchmark and probabilistic verification using Brier scores and reliability diagnostics. The temporal lag between ENSO variability and GMSTA is estimated from an initial calibration period and subsequently held fixed during retrospective evaluation and projection.

https://doi.org/10.5194/egusphere-2026-5348
Preprint. Discussion started: 7 September 2026

We apply the framework to the 2026-2027 El Niño scenario, which began on 1 August 2026, to estimate the likelihood of temporarily exceeding +1.5 °C and +2.0 °C and to quantify the projected monthly GMSTA anomaly relative to the 1850–1900 pre-industrial reference period. To assess the model-based contribution of the event to these exceedance probabilities, we compare the El Niño scenario with an ENSO-neutral counterfactual. The framework is designed to provide a transparent and repeatable assessment of how a given ENSO trajectory alters short-term global temperature projections and can be updated as new seasonal ENSO forecasts become available.

2 Data

The historical data used to train and evaluate TESR are derived from the ECMWF ERA5 reanalysis (Hersbach et al., 2020; Malardel et al., 2016), distributed through the Copernicus Climate Change Service (C3S). Monthly data are used over the period January 1940-July 2026. GMSTA are expressed relative to the pre-industrial reference period 1850–1900, while the Niño 3.4 index is calculated from ERA5 sea-surface temperature anomalies over 5°N-5°S and 170-120°W, relative to the fixed 1991-2020 climatology. The conversion of the ERA5 temperature anomalies to the 1850-1900 reference follows the C3S approach based on the difference between the two reference periods.

The Niño 3.4 index is calculated directly from ERA5, whereas the official NOAA/CPC ONI is based on ERSSTv5, in order to maintain consistency between the ENSO predictor and the temperature dataset used by TESR. The two indices represent the same underlying ENSO variability but are not expected to be identical because they rely on different datasets and processing methods.

Seasonal forecasts from BOM, CFSv2, CMCC, CanSIPS-CanESM5, CanSIPS-GEM-NEMO, DWD, ECMWF, JMA, Météo-France, NASA-GEOS-S2S-2, NCAR-CCSM4, NCAR-CESM1, and UKMO available for download from The Climate Brink ENSO Dashboard website are combined to create the ENSO scenario for the prospective period (Sect. 3.3). Using an empirical weighted-quantile approach, each forecasting system is given equal weight regardless of the size of the ensemble. Due to its strong cold bias in this scenario, which significantly impacts the lower tail of the aggregated distribution, SINTEX-F is not included in the retained ensemble.

3 Methods

3.1 TESR statistical model

TESR (Temperature–ENSO Statistical Regression) is a regularized linear regression model designed to quantify the short-term contribution of ENSO to global mean surface temperature anomalies (GMSTA). The model is formulated as

$$\mathrm{GMSTA}(t) = \beta_0 + \beta_1 t + \beta_2 t^2 + \beta_3 \mathrm{ENSO}_{\mathrm{smoothed}}(t-\tau) + \beta_4[\mathrm{ENSO}_{\mathrm{smoothed}}(t-\tau)t] + \sum_{m=2}^{12} \gamma_m I_m(t) + \varepsilon(t) \qquad (1)$$

https://doi.org/10.5194/egusphere-2026-5348
Preprint. Discussion started: 7 September 2026

where t is the number of months since the beginning of the training period, $\mathrm{ENSO}_{\mathrm{smoothed}}(t-\tau)$ is the lagged and smoothed Niño 3.4 anomaly, $I_m(t)$ denotes the monthly dummy variable for month m, and January is used as the reference month. The coefficients $\beta_0, \ldots, \beta_4$ describe the temporal and ENSO-related components, while γ_m represents the residual seasonal cycle and $\varepsilon(t)$ is the model residual.

The linear and quadratic time terms represent the evolving background temperature state, while the quadratic term allows for a non-linear change in the background warming trajectory. The interaction term between the lagged ENSO predictor and time allows the modelled sensitivity of GMSTA to ENSO to vary over the training period. These terms are included as statistical components of the model and are not interpreted individually as physically separable climate forcings.

The Niño 3.4 predictor is first smoothed using a causal three-month moving average, including the current month and the two preceding months:

$$\mathrm{ENSO}_{\mathrm{smoothed}}(t)=\frac{1}{3}\left[\mathrm{ENSO}(t)+\mathrm{ENSO}(t\text{-}1)+\mathrm{ENSO}(t\text{-}2)\right] \tag{2}$$

This causal formulation ensures that the smoothed predictor contains no information from future months. The smoothed series is subsequently shifted by a lag τ. The lag is selected from 0 to 12 months by maximizing the Pearson correlation between the lagged ENSO series and a linearly detrended GMSTA series:

$$\tau^{*}=\arg\max_{r\in\{0,\ldots,12\}}\left[\mathrm{corr}(\mathrm{ENSO}_{\mathrm{smoothed}}(t\text{-}r),\ \mathrm{GMSTA}_{\mathrm{detrended}}t)\right] \tag{3}$$

The linear detrending is applied before the correlation calculation so that the common long-term warming trend does not dominate the estimated ENSO–GMSTA relationship. This procedure gives $\tau^{*}=3$ months in the present application (r=0.39).

All continuous predictors and monthly dummy variables are standardized before fitting to avoid numerical conditioning problems associated with their different scales, particularly for the quadratic time term. For each predictor X_j, standardization is defined as

$$X_j^{*}=\frac{X_j\text{-}\overline{X_j}}{s_j}, \tag{4}$$

where $\overline{X}_j$ and s_j are the training-sample mean and standard deviation. The fitted coefficients are subsequently transformed back to the original units for interpretation and attribution. The coefficients are estimated using Ridge regression with an L_2 penalty (Hoerl and Kennard, 1970). Using the standardized design matrix $\boldsymbol{X}^{*}$, the Ridge estimator is

$$\hat{\beta}^{*}=\left(\boldsymbol{X}^{*\mathrm{T}}\boldsymbol{X}^{*}+\alpha\boldsymbol{I}\right)^{-1}\boldsymbol{X}^{*\mathrm{T}}y, \tag{5}$$

https://doi.org/10.5194/egusphere-2026-5348
Preprint. Discussion started: 7 September 2026

where $\boldsymbol{X}^*$ contains the standardized predictors, y is the vector of observed GMSTA values, α is the regularization strength, $\boldsymbol{I}$ is the identity matrix, and $\hat{\beta}^*$ is the vector of standardized regression coefficients. The regularization parameter α is selected by leave-one-out cross-validation (LOO-CV) (Stone, 1974) using the closed-form Ridge hat matrix (Golub et al., 1979),

$$\boldsymbol{H}_\alpha=\boldsymbol{X}^*\left(\boldsymbol{X}^{*\mathrm{T}}\boldsymbol{X}^*+\alpha\boldsymbol{I}\right)^{-1}\boldsymbol{X}^{*\mathrm{T}}, \tag{6}$$

For observation i, the corresponding LOO residual is obtained without repeatedly refitting the model:

$$e_{i,\mathrm{LOO}}=\frac{e_i}{1\text{-}H_{\alpha,ii}}, \tag{7}$$

where e_i is the ordinary Ridge residual. The selected regularization parameter is therefore

$$\alpha^*=\arg\min_{\alpha}\left[\frac{1}{n}\sum_{i=1}^{n}e_{i,\mathrm{LOO}}^2\right]. \tag{8}$$

This closed-form implementation provides a deterministic and reproducible hyperparameter-selection procedure and avoids repeated dependence on library-specific RidgeCV implementations.

3.2 Uncertainty estimation

Predictive uncertainty is estimated empirically from the residual structure, without imposing normally distributed and independent residuals. First, a moving block bootstrap is applied to the training residuals. Following Künsch (1989), contiguous blocks of 12 months are resampled with replacement in order to preserve short-term temporal dependence. For the fitted training model, the residuals are defined as

$$e_i=y_i\text{-}\hat{y}_i,\ i=1,\ldots,n \tag{9}$$

For a block length ℓ = 12 months, the set of available overlapping residual blocks is

$$B_s=(e_s,\ e_{s+1},\ldots,\ e_{s+l-1}),\ s=1,\ldots,\ n\text{-}l+1. \tag{10}$$

For each bootstrap replicate b, blocks are sampled independently with replacement and concatenated until a series of length n is obtained. The resulting bootstrap residual sequence is denoted $e^{*(b)}$. The synthetic response is then

$$y^{*(b)}=\hat{y}+e^{*(b)}. \tag{11}$$

Residuals are resampled in contiguous temporal blocks to preserve part of their serial dependence. A total of 1000 bootstrap

https://doi.org/10.5194/egusphere-2026-5348
Preprint. Discussion started: 7 September 2026

replicates are generated. For each replicate, the Ridge model is refitted to $\boldsymbol{X}^*$, $y^{*(b)}$ using the same value of α selected from the original training sample. The regularization parameter is therefore not re-optimized for each bootstrap realization.

The resulting bootstrap coefficients are used to recompute the ENSO-dependent component of the projection:

$$\mathrm{ENSO}^{*(b)}(t)=\beta_3^{*(b)}\mathrm{ENSO}_{\mathrm{smoothed}}(t\text{-}\tau)+\beta_4^{*(b)}\mathrm{ENSO}_{\mathrm{smoothed}}(t\text{-}r)t. \quad (12)$$

Empirical 90 % confidence intervals are obtained directly from the 5th and 95th percentiles of the resulting bootstrap distribution,

$$\mathrm{CI}_{90\,\%}(t)=\left[\mathrm{Q}_{0.05}\left(\mathrm{ENSO}^*(t)\right), \mathrm{Q}_{0.95}\left(\mathrm{ENSO}^*(t)\right)\right], \quad (13)$$

without assuming asymptotic normality of the estimator.

For the prospective 2026–2027 projections, uncertainty is propagated separately from the empirical out-of-sample residual distribution and from the multi-model ENSO scenario distribution. Individual residuals are sampled with replacement and combined with ENSO scenario draws to generate the projected temperature distribution and exceedance probabilities. This step does not use the 12-month moving-block bootstrap and therefore should not be interpreted as a full probabilistic treatment of temporal dependence. The combination of residual and ENSO-scenario uncertainty assumes that these two sources are independent. Structural uncertainty associated with alternative model specifications, parameter uncertainty not represented by the empirical residual distribution, and potential changes in the ENSO–GMSTA relationship outside the historical predictor range are not explicitly quantified.

3.3 Training and out-of-sample validation

The historical dataset is divided chronologically into an 80 % training period and a 20 % hold-out period, with no random shuffling.The Ridge penalty is selected exclusively within the training period, while the final 20 % is reserved for independent out-of-sample evaluation using correlation, R^2, and RMSE.

In addition, a walk-forward validation is performed using a rolling-origin framework (Tashman, 2000). Starting from 70 % of the available observations, the model is successively refitted at six-month intervals and used to predict the following 12 months, which are not included in the corresponding training sample. This procedure produces approximately 600 genuine out-of-sample forecast residuals and is designed to reproduce the information constraints of a pseudo-real-time forecasting setting. The Ridge penalty is kept fixed at the value selected from the original training sample.

For each forecasted observation, the genuine out-of-sample forecast residual is

https://doi.org/10.5194/egusphere-2026-5348
Preprint. Discussion started: 7 September 2026

$$e_j^{WF} = y_j - \hat{y}_j^{\mathrm{WF}}. \quad (14)$$

This procedure produces approximately 600 genuine out-of-sample forecast residuals and is designed to reproduce the information constraints of a pseudo-real-time forecasting setting, thereby avoiding the use of observations that would not have been available at the corresponding forecast origin.

These walk-forward residuals provide the empirical error distribution subsequently used for probabilistic projections. They are therefore distinct from the in-sample residuals used for the moving block bootstrap.

3.4 Prospective ENSO forcing and uncertainty propagation

The future ENSO trajectory is taken from the Climate Brink ENSO Dashboard scenario described in Sect. 4.3.1. The forecast members are processed using the same causal three-month smoothing procedure as the historical predictor and shifted by the three-month lag identified during training. The prospective experiment was defined with an initialization date of 1 August 2026; the corresponding input scenario was retrieved and archived on 10 August 2026 and compiled on 15 August 2026.

To account for uncertainty in the prescribed ENSO scenario, the individual model ensembles are combined using equal model weighting, irrespective of ensemble size, and they are not assumed to be independent. The resulting empirical distribution is represented by its minimum, 5th, 25th, 50th, 75th, 95th and maximum percentiles:

$$\mathrm{Q}(t) = [\mathrm{Q}_0, \mathrm{Q}_{0.05}, \mathrm{Q}_{0.25}, \mathrm{Q}_{0.50}, \mathrm{Q}_{0.75}, \mathrm{Q}_{0.95}, \mathrm{Q}_{1.00}]_t. \quad (15)$$

SINTEX-F is excluded from the retained ensemble because of its pronounced cold bias in the scenario considered here (Luo et al., 2005). For each projected month, 20,000 Monte Carlo ENSO values are generated from a piecewise-linear empirical quantile function defined by the percentile points above. The 20,000 Monte Carlo draws therefore increase the numerical sampling of the prescribed uncertainty distribution, but do not increase the number of independent physical forecasts represented by the multi-model ensemble. For each draw k,

$$\mathrm{ENSO}^{(k)}(t) = \mathrm{Q}^{-1}(u_k; t),\ u_k \sim \mathrm{U}(0,1), \quad (16)$$

where Q^{-1} denotes the piecewise-linear inverse quantile function defined by the available percentile points.

Each sampled ENSO trajectory is subsequently propagated through the fitted TESR model. An independently resampled walk-forward residual is then added to the corresponding central model projection:

$$\mathrm{GMSTA}^{(k)}(t) = \widehat{\mathrm{GMSTA}}_{\mathrm{TESR}}^{(k)}(t) + e^{\mathrm{WF},(k)}. \quad (17)$$

https://doi.org/10.5194/egusphere-2026-5348
Preprint. Discussion started: 7 September 2026

This procedure jointly represents uncertainty in the future ENSO trajectory and empirical model forecast error in the statistical temperature model. The two components are sampled independently and are therefore not counted twice.

The random seeds are fixed for both the bootstrap and Monte Carlo procedures to ensure exact reproducibility of the stochastic components of the analysis.

The individual seasonal prediction systems are treated as ensemble members for the purpose of constructing the empirical ENSO scenario distribution, but they are not assumed to provide statistically independent forecasts. Different systems may share observational inputs, initial conditions, assimilation products, forcing information, or model components, and their forecast errors may therefore be correlated. The resulting multi-model distribution should consequently be interpreted as an empirical representation of the spread and central tendency across available prediction systems, rather than as a collection of independent realizations. This distinction is important when propagating the distribution into the Monte Carlo experiment: the 20,000 draws do not represent 20,000 independent seasonal forecasts, but repeated numerical sampling from the empirical multi-model scenario distribution combined with the statistical-model uncertainty.

3.5 ENSO attribution and counterfactual experiment

Within TESR, the modelled global mean surface temperature can be decomposed into a background warming component and an ENSO-related component. The background warming component represents the long-term evolution of global temperature not explicitly associated with ENSO in the model, while the ENSO-related component represents the contribution of the ENSO predictors included in TESR.

Throughout this manuscript, the long-term temporal component is referred to as the “background warming component”. Given the dominant contribution of anthropogenic forcing to observed global warming over the instrumental period, this component is expected to primarily capture anthropogenic warming, while also absorbing slow-varying natural variability and other systematic effects not explicitly represented in the model. It therefore provides a first-order statistical representation of background anthropogenic warming. When interpreted in the context of the observed long-term warming trend, this component is subsequently referred to as the “anthropogenic warming component”, while not constituting a direct estimate of anthropogenic forcing or a formal detection-and-attribution result.

The contribution of ENSO is quantified using a model-based factual–counterfactual framework. The factual projection uses the prescribed ENSO scenario, whereas the counterfactual projection sets Niño 3.4 to zero throughout the projection period while keeping all other model components unchanged.

Because TESR is linear in its predictors, the difference between the factual and counterfactual projections is exactly the ENSO-dependent component:

https://doi.org/10.5194/egusphere-2026-5348
Preprint. Discussion started: 7 September 2026

$$\Delta \mathrm{ENSO}(t)=\mathrm{GMSTA}_{\mathrm{factual}}(t)-\mathrm{GMSTA}_{\mathrm{counterfactual}}(t)=\beta_3 \mathrm{ENSO}_{\mathrm{smoothed}}(t-r)+\beta_4[\mathrm{ENSO}_{\mathrm{smoothed}}(t-r)]t. \quad (18)$$

The complete model prediction can consequently be written as

$$\mathrm{GMSTA}(t)=\mathrm{Trend}(t)+\mathrm{ENSO}(t)+\mathrm{Seasonal}(t). \quad (19)$$

where

$$\mathrm{Trend}(t)=\beta_0+\beta_1 t+\beta_2 t^2, \quad (20)$$

and

$$\mathrm{ENSO}(t)=\beta_3 \mathrm{ENSO}_{\mathrm{smoothed}}(t-r)+\beta_4[\mathrm{ENSO}_{\mathrm{smoothed}}(t-r)t]. \quad (21)$$

The remaining terms constitute the background component, including the temporal trend and residual seasonal cycle. Thus, the factual–counterfactual difference is mathematically identical to the ENSO term in the model decomposition.

This counterfactual quantity represents the contribution of the ENSO predictors within TESR. It should not be interpreted as a causal physical attribution of the observed temperature anomaly, since the counterfactual is defined within the statistical model and does not represent a physically unconstrained world without ENSO.

The El Niño events of 1982-1983, 1997-1998, and 2015-2016 are treated using the same factual–counterfactual methodology. Before applying TESR to the substantially more extreme 2026-2027 scenario, these historical cases provide an out-of-sample plausibility check of the modelled ENSO contribution and its dependence on event intensity. TESR is not validated at the 2026–2027 amplitude, but its response is first evaluated through historical out-of-sample events spanning the upper part of the observed ENSO distribution. The 2026–2027 application therefore represents an extrapolation beyond the empirically tested range.

3.6 Sensitivity analysis to historical peak underestimation

A systematic tendency of TESR to underestimate the amplitude of the highest GMSTA peaks during the three strongest historical El Niño episodes (1982/83, 1997/98, and 2015/16) is found in the retrospective analysis. This behavior is in line with the ENSO predictor's three-month causal smoothing, which reduces transient maxima. The impact of this empirical peak underestimation is evaluated independently through a sensitivity analysis rather than being integrated into the central projection since the prospective 2026–2027 scenario reaches an ENSO amplitude beyond the historical calibration range.

Therefore, the goal of this analysis is to measure the sensitivity of the prospective threshold-exceedance probabilities to an additive correction of the magnitude observed at historical peaks instead of incorporating a bias correction into the primary forecast. In order to interpret the likelihood of surpassing the +1.5 °C and +2.0 °C thresholds, such an analysis offers an empirical sensitivity range.

https://doi.org/10.5194/egusphere-2026-5348
Preprint. Discussion started: 7 September 2026

For each historical El Niño episode e, the peak-underestimation bias is defined as the difference between the observed GMSTA anomaly and the corresponding TESR model estimate at the month of the observed GMSTA peak:

$$b_e = \mathrm{GMSTA_{obs}}(t_e) - \mathrm{GMSTA_{TESR}}(t_e), \quad (22)$$

where t_e represent the peak month of episode e. Positive values therefore indicate an underestimation of the observed peak amplitude by TESR.

The three historical peak biases are calculated for January 1983, February 1998 and February 2016, corresponding respectively to the 1982/83, 1997/98 and 2015/16 episodes. The empirical bias range is then defined as

$$b_{min} = \min_e (b_e),\ b_{max} = \max_e (b_e), \quad (23)$$

whereas the average historical bias is determined as

$$\bar{b} = \frac{1}{N_e} \sum_{e=1}^{N_e} b_e,\ N_e = 3. \quad (24)$$

The physically motivated sensitivity interval is derived from the resulting empirical range. TESR coefficients, ENSO lag, residual distribution, and multi-model ENSO scenario are not re-estimated.

To proceed with the propagation of the bias correction, the Monte Carlo distribution used for the potential exceedance probabilities is also used for the sensitivity analysis. Let $G_k(t)$ represent the GMSTA value from Monte Carlo realization k for a given projection month t, combining the sampled ENSO scenario and an independently resampled walk-forward model residual, as explained in Sect. 3.4.

The sensitivity-adjusted realization for a given additive peak correction b is defined as

$$G_k^{(b)}(t) = G_k(t) + b. \quad (25)$$

For a threshold T, the corresponding exceedance probability is thus

$$P_b(GMSTA(t) > T) = \frac{1}{M} \sum_{k=1}^{M} 1[G_k(t) + b > T], \quad (26)$$

where $1[\cdot]$ is the indicator function and $M = 20\,000$ is the number of Monte Carlo realizations. The effective exceedance threshold applied to the uncorrected distribution is similarly shifted by the additive correction:

$$P_b(GMSTA(t) > T) = \frac{1}{M} \sum_{k=1}^{M} 1[G_k(t) > T - b]. \quad (27)$$

https://doi.org/10.5194/egusphere-2026-5348
Preprint. Discussion started: 7 September 2026

This formulation maintains the entire structure of the original uncertainty distribution: only the amplitude of the resulting GMSTA distribution is shifted by b, leaving the ENSO multi-model dispersion and the empirical model-residual uncertainty unaltered.

With increments of 0.025 °C, the response of the prospective exceedance probabilities is assessed over a grid of additive corrections from 0 to +0.30 °C. The empirically supported range derived from the three historical peaks is represented by the interval bounded by b_{min} and b_{max}, while a continuous sensitivity curve around this range is provided by the remaining values. As an extra reference value, the central historical estimate $\overline{b}$ is presented. The sensitivity analysis is carried out for both potential thresholds, T = $+1.5\ °C$ and T = $+2.0\ °C$, as well as for the peak month of the 2026–2027 scenario. The analysis is therefore treated as a sensitivity experiment, since the central TESR projection itself is not corrected and should not be interpreted as an alternative calibrated forecast.

3.7 Retrospective forecast verification and benchmark comparison

3.7.1 Walk-forward retrospective evaluation

A rolling-origin walk-forward evaluation with an expanding training window procedure that replicates a pseudo-real-time forecasting setting while maintaining the temporal ordering of the observations is used to evaluate the retrospective predictive performance of TESR. For temporally ordered data, such out-of-sample evaluation is better than randomly shuffled cross-validation because observations at a particular forecast origin must not be influenced by later observations (Bergmeir et al., 2018).

Let t_o denote a forecast origin and D_o={$(X_t, y_t) : t \leq t_o$} the observations available at that origin. The model is fitted exclusively to D_o, yielding an origin-specific forecasting function $\hat{f}_o$. Forecasts are then generated for the subsequent H months according to

$$\hat{y}_{t_o+h|t_o}=\hat{f}_o\left(X_{t_o+h}\right),\ h=1,\ldots,H. \tag{28}$$

The corresponding forecast errors are defined as

$$e_{t_o+h|t_o}=y_{t_o+h}-\hat{y}_{t_o+h|t_o}. \tag{29}$$

The training window is progressively expanded as the forecast origin advances. In the present application, the first origin is located after 70 % of the available historical record, each subsequent origin is advanced by 6 months, and a 12-month forecast horizon is evaluated at each origin. Thus, the training sample at origin j contains all observations available before that origin, while the forecast target consists exclusively of subsequent observations. This expanding-window design

https://doi.org/10.5194/egusphere-2026-5348
Preprint. Discussion started: 7 September 2026

preserves the chronological ordering necessary for out-of-sample evaluation while enabling the model to be repeatedly recalibrated as new observations become available (Tashman, 2000). Because the 12-month forecast windows are initiated every 6 months, successive forecast windows overlap by 6 months. This overlap is retained deliberately to evaluate performance across repeated multi-month forecast horizons and is accounted for when comparing predictive accuracy between TESR and the benchmark.

For TESR, model-specific hyperparameter selection is likewise performed using only the training observations available at each origin. In particular, the Ridge regularization parameter α is reselected from the origin-specific training sample by leave-one-out cross-validation, thereby preventing subsequent observations from entering the model-fitting or hyperparameter-selection process.

3.7.2 Simple trend–ENSO benchmark

To assess whether the additional structure introduced by TESR provides predictive information beyond a conventional trend–ENSO regression, TESR is compared with a deliberately simple benchmark model inspired by the regression framework of Foster and Rahmstorf (2011). The benchmark is designed as a reference model rather than as a full reproduction of their original attribution framework and is therefore not intended to reproduce the full Foster and Rahmstorf (2011) attribution model, but to provide a deliberately parsimonious trend–ENSO baseline for predictive comparison.

For each walk-forward origin, the benchmark is fitted by ordinary least squares (OLS) using only a linear time trend and the lagged, smoothed ENSO predictor. The model can be written as

$$y_t = \beta_0 + \beta_1 t + \beta_2 E_{t-r} + \varepsilon_t, \tag{30}$$

where y_t is the GMSTA anomaly relative to the pre-industrial reference period, t is the time index, E_{t-r} is the smoothed Niño 3.4 predictor at the selected lag r, and ε_t is the residual term. The coefficients are estimated by minimizing the ordinary least-squares criterion

$$\hat{\beta} = \arg\min_{\beta} \sum_{t \in D_o} \left(y_t - \beta_0 - \beta_1 t - \beta_2 E_{t-r}\right)^2, \tag{31}$$

where D_o denotes the observations available at the corresponding forecast origin.

Unlike TESR, the benchmark contains no quadratic time term, no ENSO–time interaction, no seasonal dummy variables and no Ridge regularization. The ENSO lag is identical for TESR and the benchmark, so that the comparison does not confound model structure with differences in lag specification. The lag was selected by maximizing the correlation within the initial calibration window and then held fixed throughout the retrospective evaluation, without being re-estimated for subsequent

https://doi.org/10.5194/egusphere-2026-5348
Preprint. Discussion started: 7 September 2026

training windows. This restricted specification provides a transparent baseline against which the incremental predictive value of TESR's nonlinear temporal structure, time-varying ENSO sensitivity and regularization can be assessed.

The benchmark is assessed using the same forecast horizon, target observations, and walk-forward origins as TESR. Forecasts are then produced for the next 12 months at each origin, where the regression coefficients are only estimated from observations that were available prior to that origin. The two forecast series are aligned on their shared verification dates to ensure that differences in predictive performance reflect the model construction and not differences in the evaluation sample.

Predictive accuracy is subsequently assessed using the same deterministic verification metrics for both models, while statistical significance of differences in forecast accuracy is evaluated using the Diebold–Mariano framework described in Sect. 3.7.3.

3.7.3 Deterministic forecast verification

Deterministic predictive performance is assessed on the common set of verification dates produced by the TESR and benchmark walk-forward experiments. Because both models use the same forecast origins, forecast horizon and target observations, each TESR forecast is directly paired with a benchmark forecast for the same verification date. The comparison therefore uses paired forecast errors rather than separate test samples.

For a forecast $\hat{y}_{t|o}$ issued at origin o, the forecast error is defined as

$$e_{t|o}=y_t-\hat{y}_{t|o}. \tag{32}$$

Three complementary measures are used. The Root Mean Squared Error (RMSE) is defined as

$$RMSE=\sqrt{\frac{1}{N}\sum_{i=1}^{N} e_i^2}, \tag{33}$$

and the Mean Absolute Error (MAE) as

$$MAE=\frac{1}{N}\sum_{i=1}^{N} |e_i|. \tag{34}$$

RMSE gives greater weight to large forecast errors, whereas MAE provides a less outlier-sensitive measure of the typical absolute error. The coefficient of determination is calculated as

$$R^2=1-\frac{\sum_{i=1}^{N}(y_i-\hat{y}_i)^2}{\sum_{i=1}^{N}(y_i-\bar{y}_i)^2}, \tag{35}$$

where $\bar{y}$ is the mean of the observed GMSTA values over the common verification sample.

https://doi.org/10.5194/egusphere-2026-5348
Preprint. Discussion started: 7 September 2026

To quantify the improvement of TESR relative to the benchmark in terms of RMSE, the relative reduction is calculated as

$$\Delta RMSE=100\times\frac{RMSE_{\mathrm{benchmark}}\text{-}RMSE_{\mathrm{TESR}}}{RMSE_{\mathrm{benchmark}}}. \tag{36}$$

Because the retrospective forecasts are paired and successive 12-month forecast windows overlap due to the 6-month spacing between forecast origins, the resulting loss differentials may exhibit serial dependence. The Diebold–Mariano test is therefore implemented using a heteroskedasticity- and autocorrelation-consistent estimate of the long-run variance (Diebold and Mariano, 1995).

Using squared-error loss, the loss differential at verification time i is

$$d_i=e^2_{\mathrm{TESR},i}\text{-}e^2_{\mathrm{benchmark},i}. \tag{37}$$

The null hypothesis is that the two forecasting procedures have equal predictive accuracy, corresponding to $E(d_i)=0$. A negative mean loss differential indicates lower squared-error loss for TESR. The test statistic is constructed as

$$DM=\frac{d}{\sqrt{\mathrm{Var}(\bar{\mathrm{d}})}}, \tag{38}$$

where the long-run variance of the mean loss differential is estimated using a Newey–West heteroskedasticity- and autocorrelation-consistent estimator (Newey and West, 1987).

For the present 12-month forecast horizon, the estimator uses $H\text{-}1=11$ autocovariance lags with a Bartlett weighting kernel, thereby accounting for the serial dependence induced by overlapping forecast windows. The resulting two-sided test is evaluated at the 5 % significance level.

3.7.4 Probabilistic forecast verification

The Brier score is used to retrospectively assess probabilistic forecast performance for monthly threshold exceedances (Brier, 1950). The goal is to determine whether, when applied to observations that were not available at the time of each forecast, the probability distributions generated by TESR are instructive and suitably calibrated. The probabilistic verification uses 564 of the 600 walk-forward forecasts (with forecast origins spaced six months apart and a forecast horizon of twelve months); the first 3 forecast origins are excluded because fewer than 20 pre-origin residuals were available to build the empirical probability distribution at those dates.

For each forecast origin o, the probability that the GMSTA anomaly exceeds a threshold T is estimated from the empirical distribution obtained by adding the residuals available at that origin to the corresponding deterministic TESR prediction. This empirical residual pool contains only residuals whose target dates are strictly earlier than the forecast origin.

https://doi.org/10.5194/egusphere-2026-5348
Preprint. Discussion started: 7 September 2026

Specifically, residuals from a previous overlapping forecast window that have target dates after the current origin are not included. This keeps data from the future verification period out of the probabilistic forecast.

For a deterministic prediction $\hat{y}_{t|o}$ and an empirical residual pool $\{e_j\}_{j=1}^{M_o}$ available at origin o, the exceedance probability is therefore estimated as

$$p_{t|o}(T)=\frac{1}{M_o}\sum_{j=1}^{M_o} 1\left[\hat{y}_{t|o}+e_j>T\right]. \tag{39}$$

The realized binary outcome is

$$I_t(T)=1[y_t>T]. \tag{40}$$

Following Murphy (1973), the Brier score can be decomposed into reliability, resolution, and uncertainty components. Probabilistic accuracy is quantified using the Brier score, defined as

$$BS=\frac{1}{N}\sum_{i=1}^{N} (p_i-I_i)^2, \tag{41}$$

where p_i is the forecast probability and I_i the corresponding observed binary outcome. The Brier score ranges from zero, indicating perfect probabilistic forecasts, upward, with lower values indicating better performance (Brier, 1950).

To assess probabilistic skill relative to a climatological reference, the Brier Skill Score (BSS) is calculated as

$$BSS=1-\frac{BS_{\mathrm{TESR}}}{BS_{\mathrm{clim}}}, \tag{42}$$

The climatological reference is computed separately at each forecast origin from the observed exceedance frequency strictly preceding that origin. This ensures that the reference forecast itself does not use information from the verification period.

A reliability diagram, which contrasts the mean forecast probability within probability bins with the corresponding observed frequency, is another tool used to evaluate calibration. Forecasts that are perfectly calibrated are located on the one-to-one diagonal. Ten equally spaced probability bins are used to define the bins over the interval [0, 1]. Only bins with at least one forecast are shown. The number of forecasts in each bin determines the size of the marker.

The retrospective probabilistic verification uses a +1.0 °C threshold relative to the 1850–1900 reference period. The +1.5 °C and +2.0 °C thresholds used for the prospective 2026–2027 analysis are not suitable for this retrospective calibration experiment because they are not crossed within the historical verification sample and therefore do not provide a sufficient set of positive historical events for calibration assessment. The probabilistic verification therefore constitutes an independent

https://doi.org/10.5194/egusphere-2026-5348
Preprint. Discussion started: 7 September 2026

diagnostic of TESR's uncertainty formulation and does not validate the prospective 2026-2027 exceedance probabilities themselves.

3.8 ENSO lag selection

The temporal lag between the causally smoothed Niño 3.4 index and GMSTA was selected over a predefined range of 0-12 months by maximizing the Pearson correlation between the smoothed Niño 3.4 predictor and the detrended GMSTA series within the initial 70 % calibration window. The selected lag was then fixed throughout the subsequent walk-forward evaluation and prospective projection.

This fixed-lag strategy was adopted to provide a stable and physically interpretable temporal relationship between ENSO variability and GMSTA while avoiding the use of validation-period observations for lag selection. The same lag was used for TESR and the simple trend–ENSO benchmark to ensure a directly comparable evaluation.

The selected lag was 3 months (Pearson correlation = 0.388) in the initial 70 % calibration window.

3.9 Threshold probabilities

Probabilities of exceeding +1.5 °C and +2.0 °C relative to 1850–1900 are calculated directly from the Monte Carlo ensemble. For a threshold T, the exceedance probability for month t is defined as

$$P[\mathrm{GMSTA}(t)>T]=\frac{1}{N}\sum_{k=1}^{N} 1\left[\mathrm{GMSTA}^{(k)}>T\right]. \tag{43}$$

where $N=20\ 000$ is the number of Monte Carlo realizations and $1[\cdot]$ is the indicator function.

The same ensemble is used to derive empirical prediction intervals and probability distributions. A Gaussian kernel density estimate (KDE), using Scott's rule for bandwidth selection (Scott, 1992), is used only to provide a smoothed visualization of the empirical distributions and does not enter the calculation of exceedance probabilities.

3.10 Inter-events consistency

The factual/counterfactual decomposition is applied independently to the three historical reference episodes (1982/1983, 1997/1998, and 2015/2016), selected to span an increasing hierarchy of peak ONI intensity. Model consistency is assessed by verifying whether the estimated net ENSO contribution, expressed both in °C and as a percentage of the total anomaly, increases monotonically with peak ONI intensity across these three episodes. This provides a simple plausibility check before extrapolation to the 2026/2027 scenario, whose projected ENSO intensity exceeds that of all three historical calibration cases.

https://doi.org/10.5194/egusphere-2026-5348
Preprint. Discussion started: 7 September 2026

3.11 Model limitations

When interpreting the projections, a number of limitations should be taken into account. The extrapolation needed for the 2026-2027 scenario is the primary constraint. TESR has not been tested against predictor values similar to those anticipated during the event's strongest months because the projected ENSO amplitude is outside the historical calibration range. Additionally, the conditional ENSO-GMSTA relationship is assumed to be linear in this regime by the model. At very large ENSO amplitudes, the ENSO × time interaction does not represent nonlinear saturation or amplification, even though it permits the sensitivity to change over the historical period. If the relationship shifts outside of the observed range, the uncertainty distribution, which is also based on historical residuals, may understate structural uncertainty.

A further limitation is the restricted representation of interannual climate variability in TESR, which explicitly uses only Niño 3.4. Other potentially important sources of variability, including the Pacific Decadal Oscillation, North Atlantic variability, volcanic aerosols, and solar irradiance, are not separately represented and may therefore be partly absorbed by the background trend or residual error. The unexplained component consequently combines model error with omitted climate variability.

The ENSO scenario provided by the Climate Brink ENSO Dashboard also affects the potential probabilities. The forecast systems cannot be regarded as completely independent even though the analysis propagates the ensemble dispersion since they might share observations, initialization processes, assimilation datasets, or model components. Additional methodological decisions are introduced by equal model weighting and SINTEX-F exclusion. Certain observations that were available at initialization are not used in the final fit because the final operational coefficients are estimated from the chronological training subset, with only the most recent 20 % set aside for out-of-sample evaluation.

Internal to the statistical model, the ENSO attribution calculates the difference between the neutral counterfactual and the recommended ENSO trajectory while maintaining the same values for the other model elements. The decomposition does not uniquely partition the associated uncertainty, nor does it offer an independent physical attribution of the observed warming. Because the fixed lag was chosen from the initial 70 % calibration window rather than re-estimated within each walk-forward training window, it introduces an additional methodological limitation that could make the retrospective metrics somewhat optimistic in comparison to a fully nested procedure. Lastly, the +1.5 °C and +2.0 °C probabilities do not indicate persistent warming thresholds or tipping-point risks (Armstrong McKay et al., 2022); rather, they relate to monthly transient exceedances in relation to 1850-1900.

https://doi.org/10.5194/egusphere-2026-5348
Preprint. Discussion started: 7 September 2026

4 Results

4.1 Overall model performances

4.1.1 Walk-forward performance

TESR shows a good ability to reproduce the observed evolution of GMSTA while retaining predictive performance in out-of-sample tests. On the 20 % chronological hold-out period, the model achieves a correlation of $R=0.87$, an R^2 of 0.71 and an RMSE of 0.131 °C. The walk-forward validation, which more closely represents a pseudo-real-time forecasting setting, gives comparable performance, with an RMSE of 0.128 °C and an R^2 of 0.76 across approximately 600 genuine out-of-sample forecast residuals. The independent hold-out and walk-forward results closely agree, indicating that the model maintains significant predictive ability outside of its fitting sample. When the full hindcast is considered, the correlation reaches $R=0.949$ ($R^2=0.901$), with an RMSE of 0.129 °C. The distribution of walk-forward errors exhibits a moderate positive skewness (+0.46), indicating some asymmetry and supporting the use of an empirical, rather than purely Gaussian, representation of predictive uncertainty. Overall, these results indicate that TESR captures a substantial fraction of monthly GMSTA variability while maintaining relatively stable out-of-sample error, providing a basis for its application to the historical ENSO case studies and, subsequently, to the 2026-2027 scenario. A modest underestimation of approximately 0.1-0.2 °C is apparent during some rapid warming and cooling peaks, potentially reflecting the temporal smoothing of the ENSO predictor.

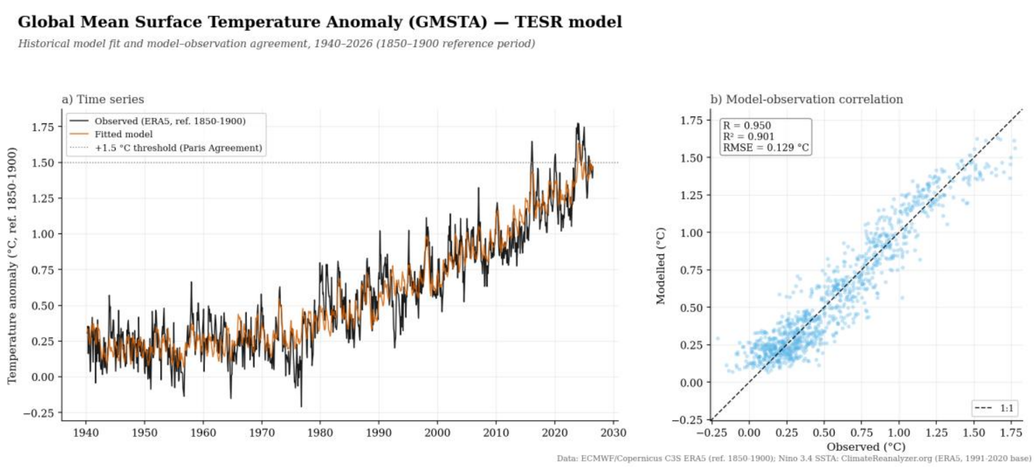

Figure 1. Historical performance of the TESR model for global mean surface temperature anomalies (GMSTA), 1940–2026. a) compares the observed GMSTA from ERA5 with the values fitted by the TESR model using the 1850–1900 reference period. b) shows the corresponding model–observation relationship, with the 1:1 line indicating perfect agreement. The +1.5 °C line indicates the Paris Agreement warming threshold relative to the 1850–1900 baseline.

https://doi.org/10.5194/egusphere-2026-5348
Preprint. Discussion started: 7 September 2026

4.1.2 TESR versus simple trend–ENSO benchmark

TESR substantially outperforms the simple trend–ENSO benchmark over the common retrospective verification period. Using the same walk-forward forecast origins, the same 12-month forecast horizon and the same fixed 3-month ENSO lag, TESR achieves an RMSE of 0.1275 °C, compared with 0.2426 °C for the benchmark, corresponding to a 47.4 % reduction in RMSE. TESR also yields a substantially lower MAE (0.1000 °C versus 0.2007 °C) and a markedly higher R^2 (0.7566 versus 0.1189; Table 1). Both models are evaluated over the same 600 forecast origins.

Model	RMSE (°C)	MAE (°C)	R^2	RMSE reduction (TESR vs benchmark)
TESR	0.1275	0.1000	0.7566	47.44 %
Benchmark (Simple trend-ENSO OLS)	0.2426	0.2007	0.1189	—

Table 1. Retrospective deterministic forecast performance of TESR and the simple trend–ENSO OLS benchmark over the common walk-forward verification period. Both models use the same forecast origins, 12-month forecast horizon and fixed 3-month ENSO lag. RMSE, MAE and R^2 are calculated from the out-of-sample forecast errors. RMSE reduction is calculated relative to the benchmark.

The improvement is statistically significant according to the Diebold–Mariano test based on squared-error loss. The resulting test statistic is DM = -6.259, with a two-sided $p<0.001$, using a Newey–West long-run variance estimate with 11 autocovariance lags. The negative sign indicates lower squared-error loss for TESR. Thus, over the retrospective verification period, the improvement in predictive accuracy is unlikely to be attributable to sampling variability alone under the null hypothesis of equal predictive accuracy.

Because the benchmark contains only a linear temporal trend and a lagged ENSO predictor, whereas TESR additionally represents nonlinear temporal evolution, an ENSO–time interaction and Ridge regularization, the comparison indicates that the additional structure incorporated into TESR provides predictive information beyond the simple trend–ENSO specification. This comparison does not establish that each individual TESR component is necessary, nor that TESR is optimal among all possible statistical formulations.

4.1.3 Probabilistic skill and reliability

Retrospective probabilistic verification further indicates substantial skill in predicting monthly exceedances of the +1.0 °C GMSTA threshold. Across 564 retrospective forecasts, generated using the same leakage-free walk-forward framework

https://doi.org/10.5194/egusphere-2026-5348
Preprint. Discussion started: 7 September 2026

described in Sect. 3.7.4, the Brier score is 0.0969, compared with 0.4794 for the corresponding per-origin climatological reference. This corresponds to a Brier Skill Score (BSS) of +0.798, indicating substantially greater probabilistic skill than the climatological reference.

The reliability diagram provides a more detailed assessment of the calibration of these probabilities (Fig. 2). Forecasts in the lower-probability range are relatively close to the one-to-one reliability line, whereas the intermediate probability bins generally lie below the diagonal, indicating that TESR tends to overestimate the observed frequency of threshold exceedance in this range. At high forecast probabilities, calibration improves substantially, with the highest-probability bin approaching the observed frequency. The reliability assessment therefore supports substantial probabilistic skill while also indicating some degree of overconfidence at intermediate probabilities.

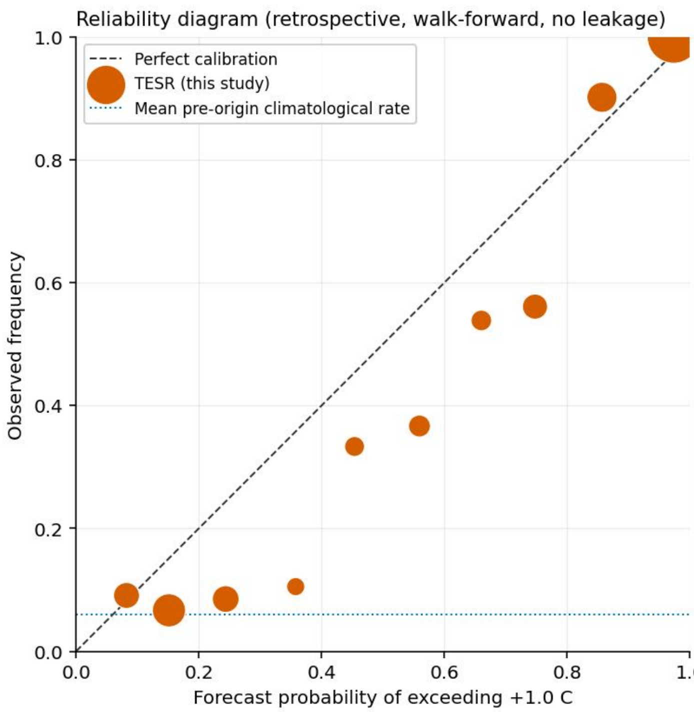

Figure 2. Reliability diagram for retrospective walk-forward predictions of monthly GMSTA exceeding +1.0 °C. Forecast probabilities were generated without access to observations occurring after each forecast origin. The diagonal denotes perfect calibration; point sizes indicate the number of forecasts in each probability bin.

These results should be interpreted as a retrospective validation of the probabilistic uncertainty framework rather than as a direct validation of the prospective 2026–2027 exceedance probabilities. The retrospective experiment uses a +1.0 °C threshold, for which a sufficient number of historical exceedances is available, whereas the prospective analysis concerns the substantially more extreme +1.5 °C and +2.0 °C thresholds. The Brier score and reliability results therefore provide evidence

https://doi.org/10.5194/egusphere-2026-5348
Preprint. Discussion started: 7 September 2026

that the empirical uncertainty formulation contains useful probabilistic information within the historical verification domain, but they do not demonstrate that probabilities at the tails of the 2026–2027 projection are perfectly calibrated.

4.2 Historical very strong El Niño events

4.2.1 1982-1983

The 1982-1983 El Niño event was the third strongest on record since 1950, with a quarterly RONI average of 2.2 °C between November 1982 and December 1983, and coincided with a global temperature that was 0.81 °C above the preindustrial baseline (GMSTA) in January 1983, a marked increase compared to the March 1982 anomaly (when ENSO transitioned from a La Niña phase to El Niño, temporarily neutral), before the onset of the episode (+0.31 °C, or +0.5 °C over 10 months in gross deviation; a check of the model's residual seasonal cycle, discussed below, explains a small portion of this).
At the peak of the atmospheric response, the model projects an anomaly range between +0.65 and +0.69 °C for GMSTA (January-May 1983), falling short of the observations by 0.05 to 0.15 °C over four of the five months, with the exception of April 1983, when the model slightly overestimates (-0.05 °C). These monthly residuals remain, in absolute terms, below or close to the model's global walk-forward RMSE (0.128 °C; Sect. 4.1), suggesting a forecast error comparable in nature to that observed out-of-sample over the entire period rather than a bias specific to this episode.

In a counterfactual world, the GMSTA would have fluctuated between 0.47 and 0.53 °C over the same period, representing a net El Niño contribution of approximately +0.21 °C [+0.17; +0.25] °C (+30 % [+26; +35] %) at the peak of its influence relative to the long-term trend (April 1983), and +0.115 °C [+0.092; +0.141] °C (+20.6 % [+17.4; +23.9] %) on average over the rolling year from July 1982 to June 1983 (Fig. 3; Table 2). Over this same annual window, the modelled anthropogenic warming component accounts for +0.53 °C (94.8 % of the total), the modelled ENSO contribution was +20.6 %, and the model's residual seasonal contribution was -15.3 % (these three terms add up exactly to the central prediction), while the share of external variability not explained by the model amounted to +0.01 °C, or less than 2 % of the average signal.

With a peak RONI of 2.2 °C, this episode provides the first point on the intensity scale sought for the inter-event consistency criterion (Sect. 3.10): its net contribution to the peak (+30 %) serves as a reference against which to compare those of the 1997/1998 and 2015/2016 episodes.

https://doi.org/10.5194/egusphere-2026-5348
Preprint. Discussion started: 7 September 2026

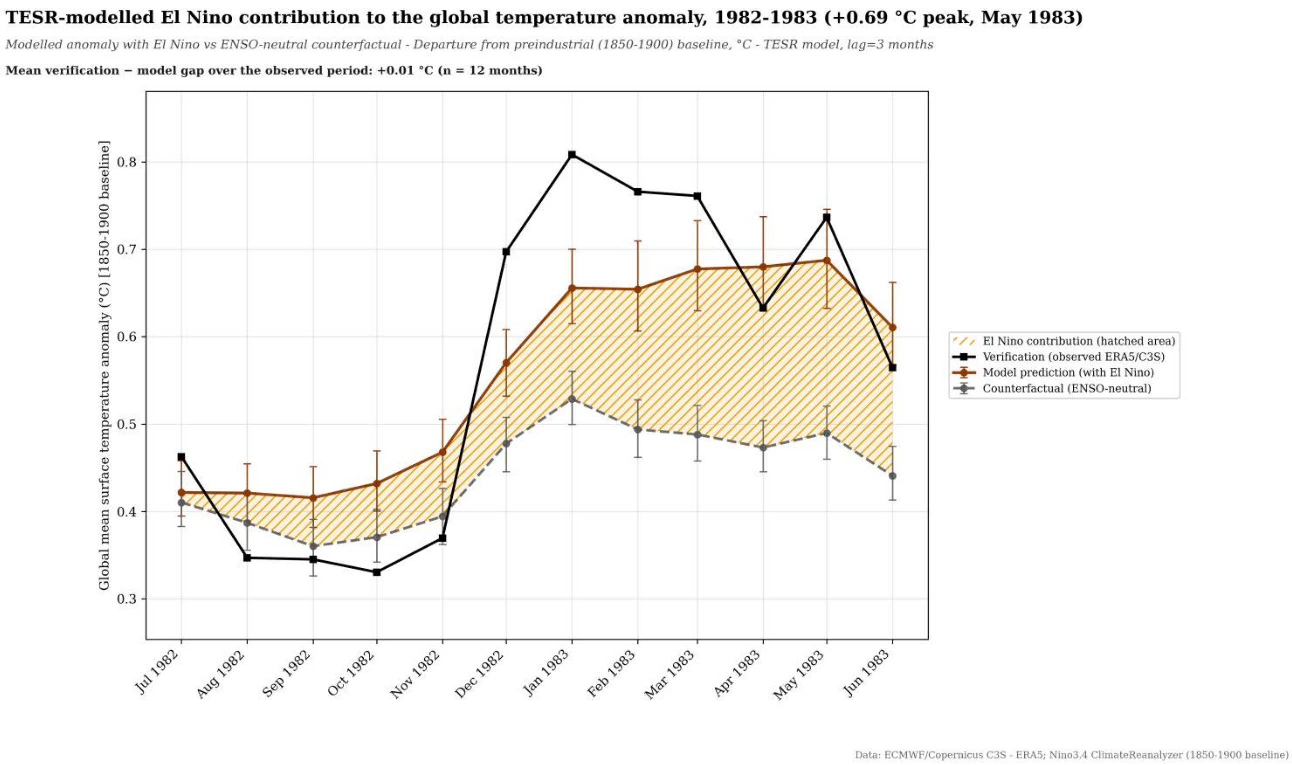

Figure 3. Counterfactual modelling of the El Niño contribution to GMSTA changes between July 1982 and June 1983.

https://doi.org/10.5194/egusphere-2026-5348
Preprint. Discussion started: 7 September 2026

Detailed monthly table - 1982-1983

TESR model - exact linear decomposition; ENSO = Model - Counterfactual (= Trend + Seasonal); Seasonal isolated separately from the Counterfactual to assess its own share; verification = ERA5/C3S observation (12/12 mois observés, réf. 1850-1900)
90% CI by moving-block bootstrap (n=300, Kunsch 1989) on all columns except Verification (fixed observation); CI of the External variability derived by symmetry of the Model's (sign reversed)
†: |%| > 100 -- Trend+Seasonal+ENSO=Total is exact in °C, but an individual % can exceed 100 (or be negative) when another component has a sign opposite to the Total (often the Seasonal term); trust the °C value in that case, not the %

Month	Model (°C)	Trend (°C | %)	Seasonal (°C | %)	Counterfactual (trend+seasonal, °C)	ENSO (°C | %)	Verification (°C)	External variability (°C | %)
Jul 1982	+0.42 °C [+0.39;+0.46] °C	+0.52 °C [+0.49;+0.55] °C +124%† [+116;+132]%	-0.11 °C [-0.14;-0.08] °C -26% [-35;-18]%	+0.41 °C [+0.38;+0.45] °C	+0.01 °C [+0.01;+0.01] °C +3% [+2;+3]%	+0.46	+0.04 °C [+0.00;+0.07] °C +10% [+1;+16]%
Aug 1982	+0.42 °C [+0.39;+0.45] °C	+0.52 °C [+0.49;+0.55] °C +124%† [+116;+133]%	-0.14 °C [-0.17;-0.11] °C -32% [-41;-24]%	+0.39 °C [+0.36;+0.42] °C	+0.03 °C [+0.03;+0.04] °C +8% [+7;+10]%	+0.35	-0.07 °C [-0.11;-0.04] °C -18% [-26;-10]%
Sep 1982	+0.42 °C [+0.38;+0.45] °C	+0.52 °C [+0.49;+0.56] °C +126%† [+118;+136]%	-0.16 °C [-0.19;-0.13] °C -39% [-49;-31]%	+0.36 °C [+0.33;+0.39] °C	+0.06 °C [+0.04;+0.07] °C +13% [+11;+16]%	+0.35	-0.07 °C [-0.11;-0.04] °C -17% [-26;-9]%
Oct 1982	+0.43 °C [+0.40;+0.47] °C	+0.53 °C [+0.50;+0.56] °C +122%† [+113;+131]%	-0.15 °C [-0.18;-0.12] °C -36% [-44;-27]%	+0.37 °C [+0.34;+0.40] °C	+0.06 °C [+0.05;+0.08] °C +14% [+12;+17]%	+0.33	-0.10 °C [-0.14;-0.07] °C -24% [-32;-16]%
Nov 1982	+0.47 °C [+0.43;+0.51] °C	+0.53 °C [+0.50;+0.56] °C +113%† [+105;+120]%	-0.13 °C [-0.16;-0.11] °C -28% [-35;-22]%	+0.39 °C [+0.36;+0.43] °C	+0.07 °C [+0.06;+0.09] °C +16% [+13;+19]%	+0.37	-0.10 °C [-0.14;-0.06] °C -21% [-29;-14]%
Dec 1982	+0.57 °C [+0.53;+0.61] °C	+0.53 °C [+0.50;+0.56] °C +93% [+87;+98]%	-0.05 °C [-0.07;-0.03] °C -9% [-13;-4]%	+0.48 °C [+0.45;+0.51] °C	+0.09 °C [+0.07;+0.11] °C +16% [+13;+19]%	+0.70	+0.13 °C [+0.09;+0.17] °C +22% [+16;+29]%
Jan 1983	+0.66 °C [+0.61;+0.70] °C	+0.53 °C [+0.50;+0.56] °C +81% [+77;+84]%	+0.00 °C [+0.00;+0.00] °C +0% [+0;+0]%	+0.53 °C [+0.50;+0.56] °C	+0.13 °C [+0.10;+0.16] °C +19% [+16;+23]%	+0.81	+0.15 °C [+0.11;+0.19] °C +23% [+17;+30]%
Feb 1983	+0.65 °C [+0.61;+0.71] °C	+0.53 °C [+0.50;+0.56] °C +81% [+75;+87]%	-0.04 °C [-0.06;-0.01] °C -6% [-10;-2]%	+0.49 °C [+0.46;+0.53] °C	+0.16 °C [+0.13;+0.20] °C +25% [+21;+28]%	+0.77	+0.11 °C [+0.06;+0.16] °C +17% [+9;+24]%
Mar 1983	+0.68 °C [+0.63;+0.73] °C	+0.53 °C [+0.50;+0.56] °C +78% [+72;+84]%	-0.04 °C [-0.07;-0.02] °C -6% [-10;-2]%	+0.49 °C [+0.46;+0.52] °C	+0.19 °C [+0.15;+0.23] °C +28% [+24;+32]%	+0.76	+0.08 °C [+0.03;+0.13] °C +12% [+4;+19]%
Apr 1983	+0.68 °C [+0.63;+0.74] °C	+0.53 °C [+0.50;+0.56] °C +78% [+72;+85]%	-0.06 °C [-0.09;-0.03] °C -9% [-14;-4]%	+0.47 °C [+0.45;+0.50] °C	+0.21 °C [+0.17;+0.25] °C +30% [+26;+35]%	+0.63	-0.05 °C [-0.10;+0.00] °C -7% [-15;+0]%
May 1983	+0.69 °C [+0.63;+0.75] °C	+0.53 °C [+0.50;+0.57] °C +78% [+72;+84]%	-0.04 °C [-0.08;-0.01] °C -6% [-12;-2]%	+0.49 °C [+0.46;+0.52] °C	+0.20 °C [+0.16;+0.24] °C +29% [+24;+33]%	+0.74	+0.05 °C [-0.01;+0.10] °C +7% [-1;+15]%
Jun 1983	+0.61 °C [+0.57;+0.66] °C	+0.53 °C [+0.51;+0.57] °C +88% [+81;+95]%	-0.09 °C [-0.13;-0.06] °C -15% [-21;-10]%	+0.44 °C [+0.41;+0.47] °C	+0.17 °C [+0.14;+0.21] °C +28% [+23;+32]%	+0.56	-0.05 °C [-0.10;-0.00] °C -8% [-16;-0]%

Data: ECMWF/Copernicus C3S - ERA5; Nino3.4 ClimateReanalyzer (ref. 1850-1900)

Table 2. Summary of the estimated impact of the modelled anthropogenic warming component, ENSO, and seasonal residual in the GMSTA evolution observed between July 1982 and June 1983, as well as the Index of Confidence (I.C.) at the 90 % threshold modeled by bootstrapping and a portion of deterministic variability not explained by the model.

4.2.2 1997-1998

With a RONI index of 2.4 °C between November 1997 and December 1998, the 1997-1998 El Niño event was the second strongest on record since 1950, behind the 2015-2016 event. The event coincided with an unprecedented rise in the GMSTA in February 1998, reaching an anomaly of +1.11 °C compared to the preindustrial era, up from +0.58 °C observed in April 1997 (before the phenomenon took hold) representing an increase of +0.53 °C in just 10 months. Between January and May 1998, the period of maximum influence of the event on the GMSTA, the model projects an anomaly ranging from +0.97 to +0.98 °C [+0.90; +1.05] °C, a modest average deviation of 0.03 °C [-0.04; +0.09] °C from the observations over the period, significantly lower than the model's average RMSE of 0.128 °C (Fig. 4; Table 3). The residuals remain close to the expected average model error, suggesting that the discrepancy is more closely related to the model's internal uncertainty than to the predominant influence of external variability.

The largest discrepancy occurred in February 1998, with the model underestimating the temperature by -0.15 °C [-0.07; -0.21] °C (-15 % [-7; -22] %) compared to observations; this was the only instance where the error was significantly above the model's expected average error. In a counterfactual world, the GMSTA would likely have fluctuated between +0.74 and +0.79 °C [+0.71; +0.83] °C over the same period, representing a net El Niño contribution of approximately +21.8 % [+17.4; +26] % on average over the period. During the warmest month (February 1998), the model estimates that ENSO accounted for +0.21 °C [+0.16; +0.27] °C of this increase, or +22 % [+17; +26] %. At the peak of El Niño's influence on the GMSTA, relative to the long-term trend in April 1998, its estimated contribution was 0.23 °C [+0.17; +0.29] °C, or +23 % [+19; +28] %. On average over the rolling 12-month period from July 1997 to June 1998, the modelled anthropogenic warming component accounted for +0.79 °C [+0.76; +0.82] °C (+93.7 % [+88.6; +98.8] %) of the balance, the modelled ENSO

https://doi.org/10.5194/egusphere-2026-5348
Preprint. Discussion started: 7 September 2026

contribution was +0.14 °C [+0.1; +0.18] °C (+16.4 % [+12.4; +20.1] %), and the model's residual seasonal contribution was -0.09 °C [-0.1; -0.07] °C (-10.1 % [-12.4; -7.8] %), while the share of unexplained external variability amounts to +0.04 °C, or +4.4 % of the average signal (Table 2).

Compared to the 1982–1983 episode over the same annual period (background warming component +0.53 °C [+0.50; +0.56] °C, or +94.6 % [+89.1; +100.4] % of the total; ENSO +0.11 °C [+0.09; +0.14] °C, or +20.6 % [+16.6; +24.1] %; residual seasonal component -0.08 °C [-0.10; -0.07] °C, or -15.3 % [-18.9; -11.7] %; external variability +0.01 °C, or +1.9 % over the 12 observed months), the relative contribution of ENSO to the 1997/1998 annual balance appears to have declined by approximately -4.3 % (16.3 % versus 20.6 %), and the residual seasonal component is less negative at +5.2 % (-10.1 % versus -15.3 %), even though the RONI intensity of the episode is higher (+0.2 °C, or +9 %: 2.4 °C versus 2.2 °C) and the modelled anthropogenic warming component was higher in absolute terms by +0.27 °C (from +0.53 °C to +0.79 °C). These differences between episodes relate to the central estimates (bootstrap medians) of each independent decomposition (they do not themselves constitute a joint confidence interval, which would require a paired bootstrap analysis of both episodes simultaneously). This finding is consistent with an ENSO contribution to GMSTA that is increasingly overshadowed, for comparable RONI intensities, by a background warming component associated primarily with the long-term anthropogenic warming trend.

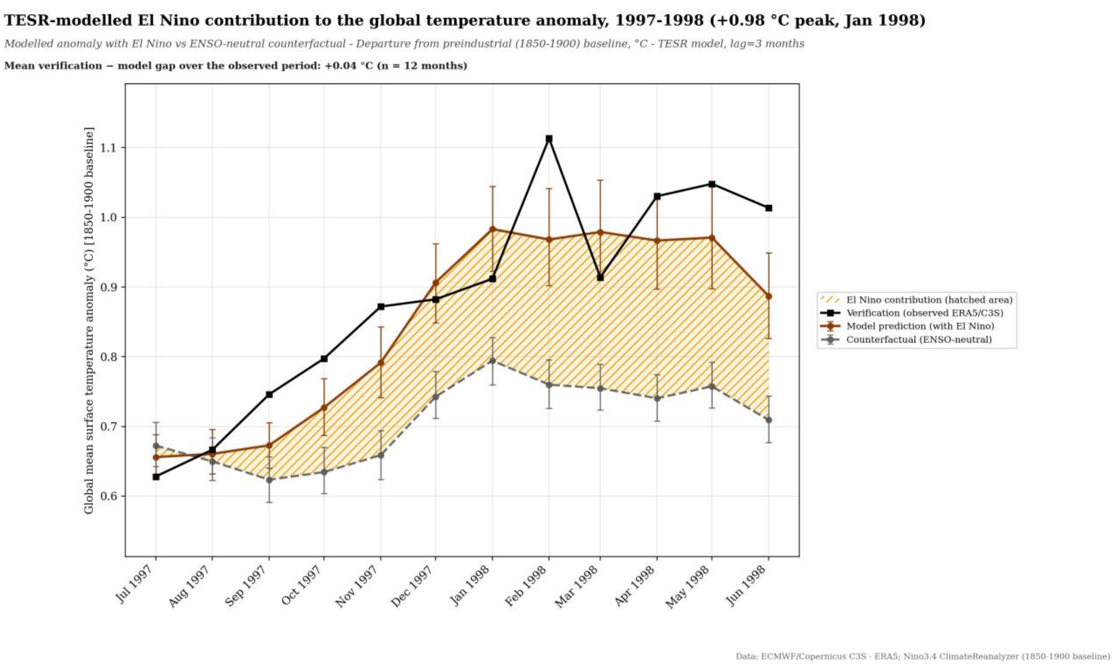

Figure 4. Counterfactual modelling of the El Niño contribution to GMSTA changes between July 1997 and June 1998.

.

https://doi.org/10.5194/egusphere-2026-5348
Preprint. Discussion started: 7 September 2026

Detailed monthly table - 1997-1998

TESR model - exact linear decomposition; ENSO = Model - Counterfactual (= Trend + Seasonal); Seasonal isolated separately from the Counterfactual to assess its own share; verification = ERA5/C3S observation (12/12 mois observés, réf. 1850-1900)
90% CI by moving-block bootstrap (n=300, Kunsch 1989) on all columns except Verification (fixed observation); CI of the External variability derived by symmetry of the Model's (sign reversed)
†: |%| > 100 -- Trend+Seasonal+ENSO=Total is exact in °C, but an individual % can exceed 100 (or be negative) when another component has a sign opposite to the Total (often the Seasonal term); trust the °C value in that case, not the %

Month	Model (°C)	Trend (°C | %)	Seasonal (°C | %)	Counterfactual (trend+seasonal, °C)	ENSO (°C | %)	Verification (°C)	External variability (°C | %)
Jul 1997	+0.66 °C [+0.63;+0.69] °C	+0.78 °C [+0.75;+0.82] °C +119%† [+114;+125]%	-0.11 °C [-0.14;-0.08] °C -17% [-22;-12]%	+0.67 °C [+0.64;+0.71] °C	-0.02 °C [-0.02;-0.01] °C -3% [-3;-2]%	+0.63	-0.03 °C [-0.06;+0.00] °C -4% [-9;+0]%
Aug 1997	+0.66 °C [+0.63;+0.70] °C	+0.79 °C [+0.75;+0.82] °C +119%† [+114;+124]%	-0.14 °C [-0.17;-0.11] °C -21% [-26;-16]%	+0.65 °C [+0.62;+0.68] °C	+0.01 °C [+0.01;+0.01] °C +2% [+1;+2]%	+0.67	+0.01 °C [-0.03;+0.03] °C +1% [-4;+5]%
Sep 1997	+0.67 °C [+0.64;+0.71] °C	+0.79 °C [+0.75;+0.82] °C +117%† [+112;+122]%	-0.16 °C [-0.19;-0.13] °C -24% [-30;-20]%	+0.62 °C [+0.59;+0.66] °C	+0.05 °C [+0.04;+0.06] °C +7% [+6;+9]%	+0.75	+0.07 °C [+0.04;+0.11] °C +11% [+6;+16]%
Oct 1997	+0.73 °C [+0.69;+0.77] °C	+0.79 °C [+0.76;+0.82] °C +109%† [+103;+114]%	-0.15 °C [-0.18;-0.12] °C -21% [-26;-16]%	+0.63 °C [+0.60;+0.67] °C	+0.09 °C [+0.07;+0.12] °C +13% [+10;+16]%	+0.80	+0.07 °C [+0.03;+0.11] °C +10% [+4;+15]%
Nov 1997	+0.79 °C [+0.74;+0.84] °C	+0.79 °C [+0.76;+0.82] °C +100% [+94;+105]%	-0.13 °C [-0.16;-0.11] °C -17% [-21;-13]%	+0.66 °C [+0.62;+0.69] °C	+0.13 °C [+0.10;+0.17] °C +17% [+13;+20]%	+0.87	+0.08 °C [+0.03;+0.13] °C +10% [+4;+17]%
Dec 1997	+0.91 °C [+0.85;+0.96] °C	+0.79 °C [+0.76;+0.83] °C +87% [+82;+93]%	-0.05 °C [-0.07;-0.03] °C -6% [-8;-3]%	+0.74 °C [+0.71;+0.78] °C	+0.16 °C [+0.12;+0.21] °C +18% [+14;+22]%	+0.88	-0.02 °C [-0.08;+0.03] °C -3% [-9;+4]%
Jan 1998	+0.98 °C [+0.92;+1.04] °C	+0.79 °C [+0.76;+0.83] °C +81% [+77;+85]%	+0.00 °C [+0.00;+0.00] °C +0% [+0;+0]%	+0.79 °C [+0.76;+0.83] °C	+0.19 °C [+0.14;+0.24] °C +19% [+15;+23]%	+0.91	-0.07 °C [-0.13;-0.01] °C -7% [-13;-1]%
Feb 1998	+0.97 °C [+0.90;+1.04] °C	+0.80 °C [+0.76;+0.83] °C +82% [+76;+87]%	-0.04 °C [-0.06;-0.01] °C -4% [-6;-1]%	+0.76 °C [+0.73;+0.80] °C	+0.21 °C [+0.16;+0.27] °C +22% [+17;+26]%	+1.11	+0.15 °C [+0.07;+0.21] °C +15% [+7;+22]%
Mar 1998	+0.98 °C [+0.91;+1.05] °C	+0.80 °C [+0.76;+0.83] °C +81% [+75;+87]%	-0.04 °C [-0.07;-0.02] °C -4% [-7;-2]%	+0.75 °C [+0.72;+0.79] °C	+0.22 °C [+0.17;+0.29] °C +23% [+18;+27]%	+0.91	-0.07 °C [-0.14;+0.00] °C -7% [-14;+0]%
Apr 1998	+0.97 °C [+0.90;+1.03] °C	+0.80 °C [+0.76;+0.83] °C +83% [+77;+89]%	-0.06 °C [-0.09;-0.03] °C -6% [-9;-3]%	+0.74 °C [+0.71;+0.77] °C	+0.23 °C [+0.17;+0.29] °C +23% [+19;+28]%	+1.03	+0.06 °C [-0.00;+0.13] °C +7% [-0;+14]%
May 1998	+0.97 °C [+0.90;+1.05] °C	+0.80 °C [+0.77;+0.83] °C +83% [+77;+89]%	-0.04 °C [-0.08;-0.01] °C -5% [-8;-1]%	+0.76 °C [+0.73;+0.79] °C	+0.21 °C [+0.16;+0.27] °C +22% [+18;+26]%	+1.05	+0.08 °C [+0.00;+0.15] °C +8% [+0;+15]%
Jun 1998	+0.89 °C [+0.83;+0.95] °C	+0.80 °C [+0.77;+0.84] °C +91% [+85;+97]%	-0.09 °C [-0.13;-0.06] °C -11% [-14;-7]%	+0.71 °C [+0.68;+0.74] °C	+0.18 °C [+0.13;+0.23] °C +20% [+16;+24]%	+1.01	+0.13 °C [+0.06;+0.19] °C +14% [+7;+21]%

Data: ECMWF/Copernicus C3S - ERA5; Nino3.4 ClimateReanalyzer (ref. 1850-1900)

Table 3. Recapitulative of the estimated impact of the modelled anthropogenic warming component, ENSO, and seasonal residual in the GMSTA evolution observed between July 1997 and June 1998, as well as the Index of Confidence (I.C.) at the 90 % threshold modeled by bootstrapping and a portion of deterministic variability not explained by the model.

4.2.3 2015-2016

The 2015-2016 El Niño event, which peaked during the NDJ quarter of 2015 with a RONI index of 2.8 °C, remains to this day the most intense El Niño event ever recorded since the beginning of modern observations in 1950, and was marked by the crossing of the +1.5 °C threshold set by the Paris Agreement relative to pre-industrial levels for the first time in modern observational history between January and March 2016, reaching as high as +1.65 °C in February 2016, and also becoming the hottest year on record (+1.31 °C), far surpassing the previous record set in 2010 (+1 °C). With a GMSTA of +1.18 °C in March 2015, before the phenomenon began, this represents a rise in global temperatures of +0.47 °C over 11 months—more modest than during the 1997-1998 event but greater than in 1982-1983. As with the two previous very strong El Niño events studied earlier, the maximum influence projected by the TESR model on the GMSTA occurs between January and May 2016 (Fig. 5), with a projected anomaly between +1.42 and +1.43 °C [+1.3; +1.55] °C over the period, with an average deviation of +0.06 °C [-0.05; +0.17] °C (Table 4), slightly higher than that of the 1997/1998 episode (Fig. 4). In a counterfactual world, the GMSTA would likely have fluctuated between +1.19 and +1.24 °C [+1.12; +1.32] °C.

Over this period, the ENSO contribution to the change in GMSTA is estimated to be between +0.19 and +0.23 °C [+0.12; +0.32] °C, so +13 to +16 % [+9; +21] %, down from the two previous events, due to a greater modelled anthropogenic warming component in the global heat balance. In February 2016, when the largest deviation from the model was observed (+0.22 °C [+0.11; +0.33] °C), which was also the warmest month of the period, the ENSO contribution to this warming is estimated by the model at +0.21 °C [+0.13; +0.3] °C, representing a 15 % [+10; +20] % share, whereas the peak of ENSO influence on the GMSTA occurs between March and April 2016 in the model, where it accounts for +0.23 °C [+0.14; +0.32] °C, representing a contribution of +16 % [10; +21] %, a time window similar to that of the 1982/83 and 1997/98

https://doi.org/10.5194/egusphere-2026-5348
Preprint. Discussion started: 7 September 2026

events, and a marked decrease compared to previous peaks (Fig. 17). On average over the rolling 12-month period from July 2015 to June 2016, the model's decomposition attributes +1.24 °C [+1.16; +1.32] °C to the modelled background anthropogenic warming component, representing +95.1 % [+90.4; +100.1] % of the average balance; ENSO +0.15 °C [+0.09; +0.21] °C, or +11.5 % [+7.1; +15.5] %; and the model's residual seasonal component -0.08 °C [-0.10; -0.07] °C, or -6.5 % [-8.1; -5.0] % (these three terms add up exactly to the central prediction, +1.31 °C [+1.21; +1.41] °C, over this same time window; Table 4). The portion of external variability not explained by the model (deterministic verification-model difference, which cannot be bootstrapped in the same way as the three previous components) is virtually zero on an annual average: -0.004 °C over the 12 observed months, or -0.3 % of the average signal (the monthly deviations, notably the peak of +0.22 °C in February 2016, almost entirely offset each other over the course of the year).

Compared to the two previous episodes over the same annual window (trend of +0.53 °C for 1982/83, +0.79 °C for 1997/98, +1.24 °C for 2015/2016), the relative contribution of ENSO to the annual balance continues to decline, a trend that began in 1997/98: +20.6 % in 1982/83, +16.3 % in 1997/98, +11.5 % in 2015/2016 (i.e., -4.8 % compared to 1997/98 and -9.1 percentage points compared to 1982/83), while the residual seasonal component is also decreasing in relative terms (-15.3 % → –10.1 % → –6.5 %, or +3.6 and +8.8 percentage points, respectively). This gradual reduction in the ENSO and seasonal residual components of the balance, as the background anthropogenic warming trend increases in absolute magnitude (+0.53 °C → +0.79 °C → +1.24 °C), is consistent for this third episode (the most intense in the series with a RONI of 2.8 °C) with the same dynamic already observed between 1982/83 and 1997/98: El Niño's influence on the GMSTA is relatively diminishing, not because ENSO is weakening in physical intensity, but because the denominator (the background trend) is growing faster than its absolute contribution. As before, these cross-episode comparisons are based on independent central estimates, not on a joint interval.

https://doi.org/10.5194/egusphere-2026-5348
Preprint. Discussion started: 7 September 2026

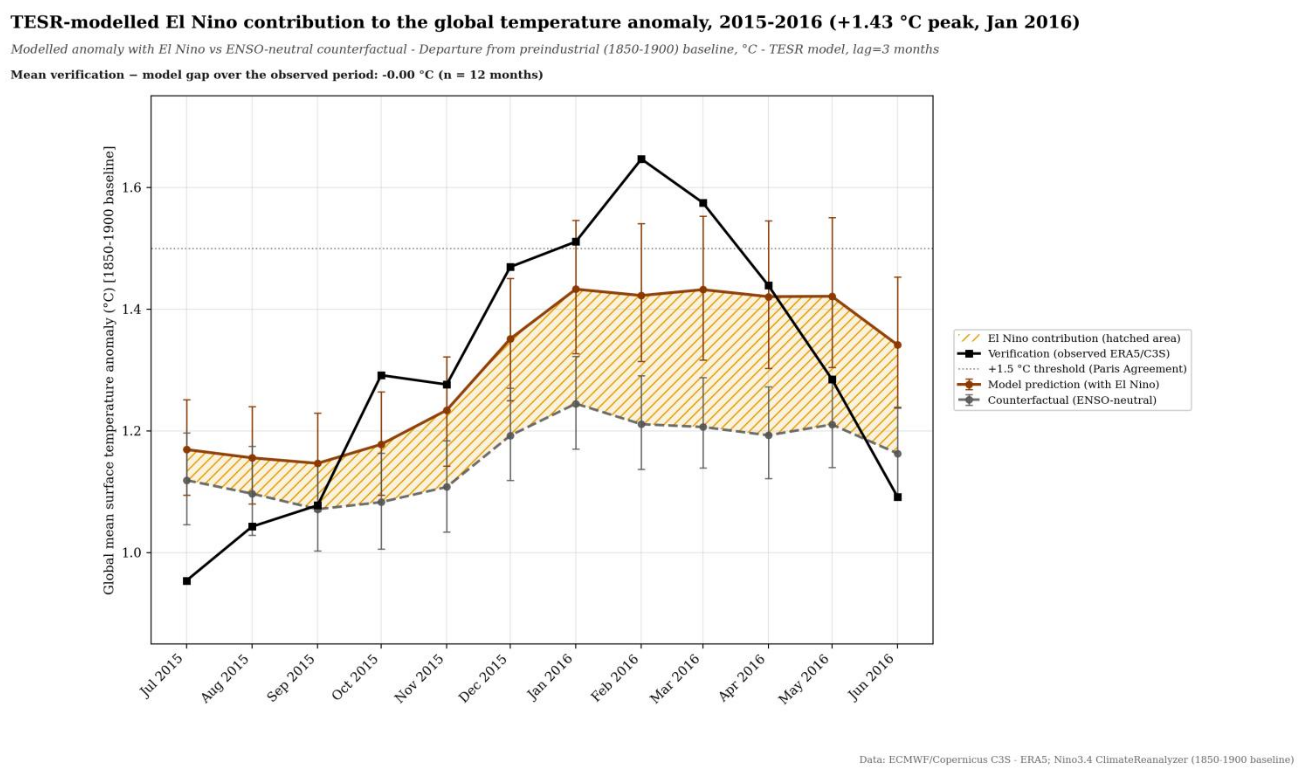

Figure 5. Counterfactual modelling of the El Niño contribution to GMSTA changes between July 2015 and June 2016.

Detailed monthly table - 2015-2016

TESR model - exact linear decomposition; ENSO = Model - Counterfactual (= Trend + Seasonal); Seasonal isolated separately from the Counterfactual to assess its own share; verification = ERA5/C3S observation (12/12 mois observés, réf. 1850-1900)
90% CI by moving-block bootstrap (n=300, Kunsch 1989) on all columns except Verification (fixed observation); CI of the External variability derived by symmetry of the Model's (sign reversed)
†: |%| > 100 -- Trend+Seasonal+ENSO=Total is exact in °C, but an individual % can exceed 100 (or be negative) when another component has a sign opposite to the Total (often the Seasonal term); trust the °C value in that case, not the %

Month	Model (°C)	Trend (°C | %)	Seasonal (°C | %)	Counterfactual (trend+seasonal, °C)	ENSO (°C | %)	Verification (°C)	External variability (°C | %)
Jul 2015	+1.17 °C [+1.09;+1.25] °C	+1.23 °C [+1.16;+1.31] °C +105%† [+102;+109]%	-0.11 °C [-0.14;-0.08] °C -10% [-13;-7]%	+1.12 °C [+1.05;+1.20] °C	+0.05 °C [+0.03;+0.07] °C +4% [+3;+6]%	+0.95	-0.22 °C [-0.30;-0.14] °C -18% [-25;-12]%
Aug 2015	+1.16 °C [+1.08;+1.24] °C	+1.23 °C [+1.16;+1.31] °C +107%† [+103;+110]%	-0.14 °C [-0.17;-0.11] °C -12% [-15;-9]%	+1.10 °C [+1.03;+1.17] °C	+0.06 °C [+0.04;+0.08] °C +5% [+3;+7]%	+1.04	-0.11 °C [-0.20;-0.04] °C -10% [-17;-3]%
Sep 2015	+1.15 °C [+1.07;+1.23] °C	+1.24 °C [+1.16;+1.31] °C +108%† [+104;+112]%	-0.16 °C [-0.19;-0.13] °C -14% [-17;-12]%	+1.07 °C [+1.00;+1.15] °C	+0.08 °C [+0.05;+0.11] °C +7% [+4;+9]%	+1.08	-0.07 °C [-0.15;+0.01] °C -6% [-13;+1]%
Oct 2015	+1.18 °C [+1.09;+1.26] °C	+1.24 °C [+1.16;+1.32] °C +105%† [+101;+110]%	-0.15 °C [-0.18;-0.12] °C -13% [-16;-10]%	+1.08 °C [+1.01;+1.16] °C	+0.09 °C [+0.06;+0.13] °C +8% [+5;+11]%	+1.29	+0.11 °C [+0.03;+0.20] °C +10% [+2;+17]%
Nov 2015	+1.23 °C [+1.14;+1.32] °C	+1.24 °C [+1.17;+1.32] °C +100%† [+96;+105]%	-0.13 °C [-0.16;-0.11] °C -11% [-13;-8]%	+1.11 °C [+1.03;+1.18] °C	+0.13 °C [+0.08;+0.18] °C +10% [+7;+14]%	+1.28	+0.04 °C [-0.05;+0.13] °C +3% [-4;+11]%
Dec 2015	+1.35 °C [+1.25;+1.45] °C	+1.24 °C [+1.17;+1.32] °C +92% [+87;+97]%	-0.05 °C [-0.07;-0.03] °C -4% [-5;-2]%	+1.19 °C [+1.12;+1.27] °C	+0.16 °C [+0.10;+0.22] °C +12% [+8;+16]%	+1.47	+0.12 °C [+0.02;+0.22] °C +9% [+1;+16]%
Jan 2016	+1.43 °C [+1.33;+1.55] °C	+1.24 °C [+1.17;+1.32] °C +87% [+82;+91]%	+0.00 °C [+0.00;+0.00] °C +0% [+0;+0]%	+1.24 °C [+1.17;+1.32] °C	+0.19 °C [+0.12;+0.26] °C +13% [+9;+18]%	+1.51	+0.08 °C [-0.04;+0.18] °C +5% [-2;+13]%
Feb 2016	+1.42 °C [+1.31;+1.54] °C	+1.25 °C [+1.17;+1.33] °C +88% [+82;+93]%	-0.04 °C [-0.06;-0.01] °C -3% [-4;-1]%	+1.21 °C [+1.14;+1.29] °C	+0.21 °C [+0.13;+0.30] °C +15% [+10;+20]%	+1.65	+0.22 °C [+0.11;+0.33] °C +16% [+7;+23]%
Mar 2016	+1.43 °C [+1.32;+1.55] °C	+1.25 °C [+1.17;+1.33] °C +87% [+82;+93]%	-0.04 °C [-0.07;-0.02] °C -3% [-5;-1]%	+1.21 °C [+1.14;+1.29] °C	+0.23 °C [+0.14;+0.32] °C +16% [+10;+21]%	+1.58	+0.14 °C [+0.02;+0.26] °C +10% [+2;+18]%
Apr 2016	+1.42 °C [+1.30;+1.55] °C	+1.25 °C [+1.18;+1.33] °C +88% [+82;+95]%	-0.06 °C [-0.09;-0.03] °C -4% [-6;-2]%	+1.19 °C [+1.12;+1.27] °C	+0.23 °C [+0.14;+0.32] °C +16% [+11;+21]%	+1.44	+0.02 °C [-0.11;+0.14] °C +1% [-8;+10]%
May 2016	+1.42 °C [+1.30;+1.55] °C	+1.25 °C [+1.18;+1.33] °C +88% [+83;+95]%	-0.04 °C [-0.08;-0.01] °C -3% [-5;-1]%	+1.21 °C [+1.14;+1.29] °C	+0.21 °C [+0.13;+0.30] °C +15% [+10;+20]%	+1.28	-0.14 °C [-0.27;-0.02] °C -10% [-19;-1]%
Jun 2016	+1.34 °C [+1.24;+1.45] °C	+1.26 °C [+1.18;+1.34] °C +94% [+88;+100]%	-0.09 °C [-0.13;-0.06] °C -7% [-10;-5]%	+1.16 °C [+1.09;+1.24] °C	+0.18 °C [+0.11;+0.25] °C +13% [+9;+18]%	+1.09	-0.25 °C [-0.36;-0.15] °C -19% [-27;-11]%

Data: ECMWF/Copernicus C3S · ERA5; Nino3.4 ClimateReanalyzer (ref. 1850-1900)

Table 4. Recapitulative of the estimated impact of the modelled anthropogenic warming component, ENSO, and seasonal residual in the GMSTA evolution observed between July 2015 and June 2016, as well as the Index of Confidence (I.C.) at the 90 % threshold modeled by bootstrapping and a portion of deterministic variability not explained by the model.

https://doi.org/10.5194/egusphere-2026-5348
Preprint. Discussion started: 7 September 2026

4.3 Model projection for the Record-Breaking 2026-2027 El Niño

4.3.1 ENSO trajectory hypothesis

The scenarios used to develop projections for the period July 2026-August 2027 are based on C3S seasonal models initialized on 1 August 2026, in the Niño 3.4 region relative to the 1991-2020 climatological baseline, covering the period from August 2026 - April 2027, allowing for a projection through August 2027 based on the previously identified optimal 3-month lag. The central scenario is derived from the multi-model median, as compiled by The Climate Brink website, along with their adjacent envelopes Q25-Q75, Q5-Q95, and Q0-Q100. Probabilities are adjusted according to the quantile indicating the extent to which each hypothesis is represented in the ensembles.

Fig. 6 illustrates the construction of this central scenario. The multi-model median of the ONI/Niño 3.4 index (equal weighting per model, excluding SINTEX-F) rises almost continuously from January 2026, peaking at +3.96 °C in November 2026, before falling to +3.92 °C in December 2026 and then to +2.30 °C in April 2027 (Table 5). The three historical analogs selected for comparison (1982/83, 1997/98, 2015/2016) appear significantly lower throughout the entire period, each peaking between +2.6 °C and +2.8 °C, which visually underscores the unprecedented nature of the 2026/2027 scenario already highlighted in the Introduction. The projected intensity of the ONI peak (multi-model median of +3.96 °C in November 2026, Fig. 7) places this event outside the entire range of ENSO variability observed since 1950: the multi-model distribution for the month of peak intensity (Fig. 7) shows a concentration of probability between +3.5 °C and +4.5 °C (more than 65 % of the weighted members fall within this interval), with a significant upper tail beyond +4.5 °C (≈ 7 % of the members) and a virtually empty lower tail below +3.0 °C (≈ 3.5 %), an asymmetry that underscores that the risk, in this distribution, leans toward values even more extreme than the median rather than toward a possible early tailing off of the episode.

https://doi.org/10.5194/egusphere-2026-5348
Preprint. Discussion started: 7 September 2026

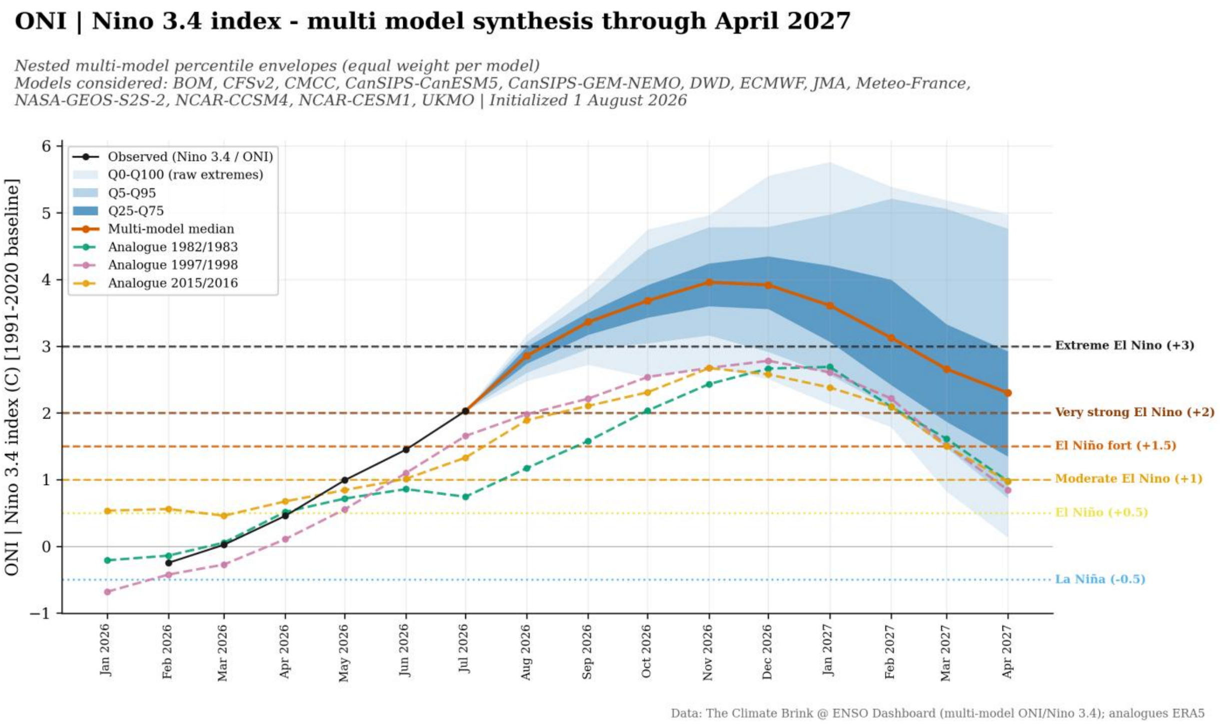

Figure 6. Multi-model synthesis of the ONI/Niño 3.4 index through April 2027 (nested percentile envelopes, equal weighting per model) initialized on 1 August 2026, compared to the three historical analogs: 1982/83, 1997/98, and 2015/2016. Data: The Climate Brink @ ENSO Dashboard; ERA5 analogs.

https://doi.org/10.5194/egusphere-2026-5348
Preprint. Discussion started: 7 September 2026

Official ONI forecast (member-level multi-model distribution)

August 2026-April 2027 - official multi-model scenario (Climate Dashboard), initialized 1 August 2026 - member-level quantiles - ONI / Nino 3.4 index, 1991-

Month	Median (ONI, °C)	Q25-Q75 (°C)	Q5-Q95 (°C)	Q0-Q100 (°C)
Aug 2026	+2.86 °C	[+2.74; +2.99]	[+2.60; +3.07]	[+2.48; +3.17]
Sep 2026	+3.36 °C	[+3.17; +3.50]	[+2.96; +3.70]	[+2.72; +3.89]
Oct 2026	+3.68 °C	[+3.43; +3.92]	[+3.04; +4.45]	[+2.54; +4.75]
Nov 2026	+3.96 °C	[+3.60; +4.24]	[+3.16; +4.78]	[+2.69; +4.96]
Dec 2026	+3.92 °C	[+3.56; +4.35]	[+2.92; +4.79]	[+2.51; +5.55]
Jan 2027	+3.61 °C	[+3.07; +4.21]	[+2.57; +4.98]	[+2.13; +5.76]
Feb 2027	+3.13 °C	[+2.42; +4.00]	[+2.08; +5.21]	[+1.79; +5.39]
Mar 2027	+2.66 °C	[+1.87; +3.33]	[+1.48; +5.06]	[+0.82; +5.19]
Apr 2027	+2.30 °C	[+1.35; +2.92]	[+0.72; +4.76]	[+0.13; +4.97]

Data: The Climate Brink @ ENSO Dashboard (member-level multi-model distribution)

Table 5. Official multi-model ONI forecast for August 2026–April 2027. Monthly median values and Q25–Q75, Q5–Q95, and Q0–Q100 uncertainty ranges calculated from the retained member-level Climate Dashboard data using equal weighting by model and does not represent the original member-by-member model distribution. ONI values are relative to the 1991–2020 baseline.

https://doi.org/10.5194/egusphere-2026-5348
Preprint. Discussion started: 7 September 2026

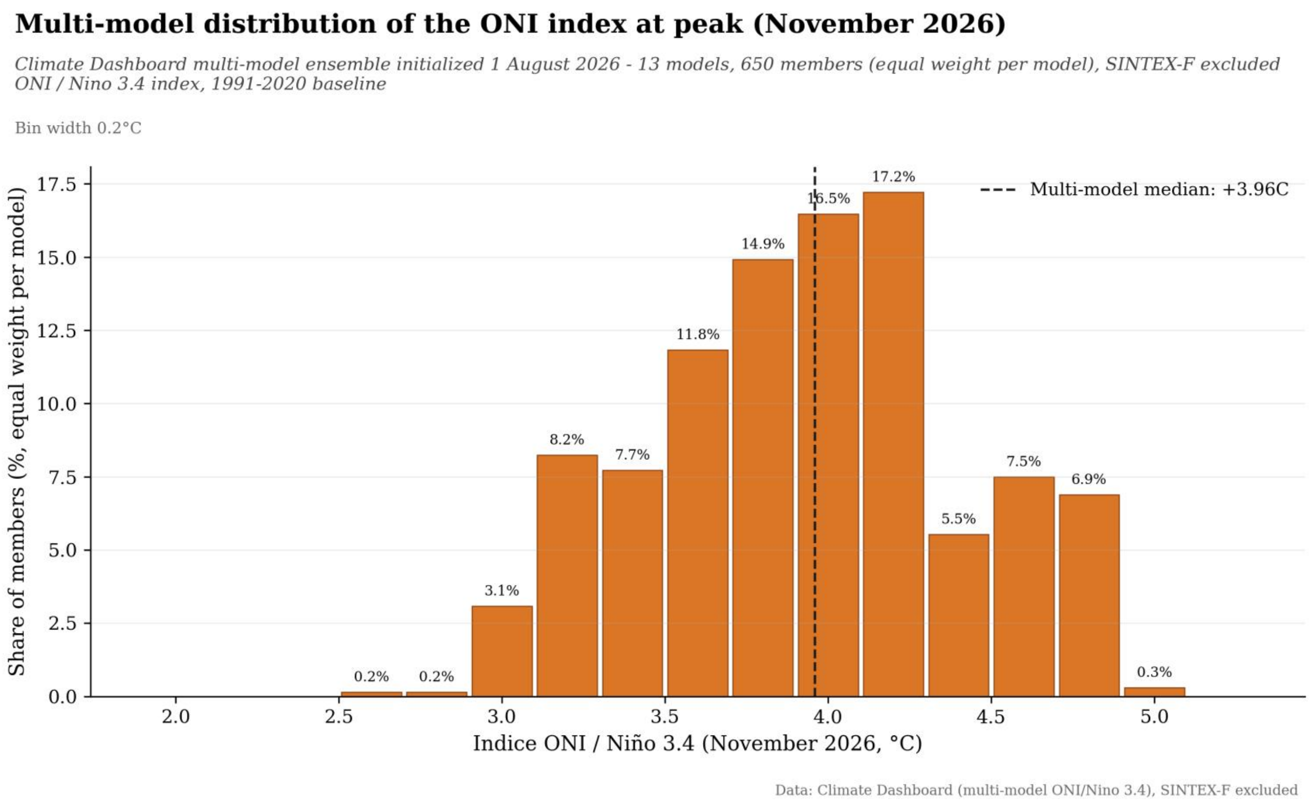

Figure 7. Multi-model distribution of the ONI/Niño 3.4 index during the scenario's peak month (November 2026), initialized on 1 August 2026, 0.2 °C resolution, equal weighting by model, excluding SINTEX-F. Multi-model median: +3.96 °C. Data: Climate Dashboard (ONI/Niño 3.4 multi-model), excluding SINTEX-F.

4.3.2 Forecast for July 2026 - August 2027 period

A first verification point became available after the initial characterization of the ENSO scenario: the observed July 2026 GMSTA anomaly from ERA5/C3S was +1.47 °C, exactly matching the modelled value for the same month (Figs. 8-9), without any re-estimation of the model coefficients. A single out-of-sample month is, of course, insufficient to assess the reliability of the full projection period, but this agreement provides an initial consistency check at the beginning of the forecast window.

https://doi.org/10.5194/egusphere-2026-5348
Preprint. Discussion started: 7 September 2026

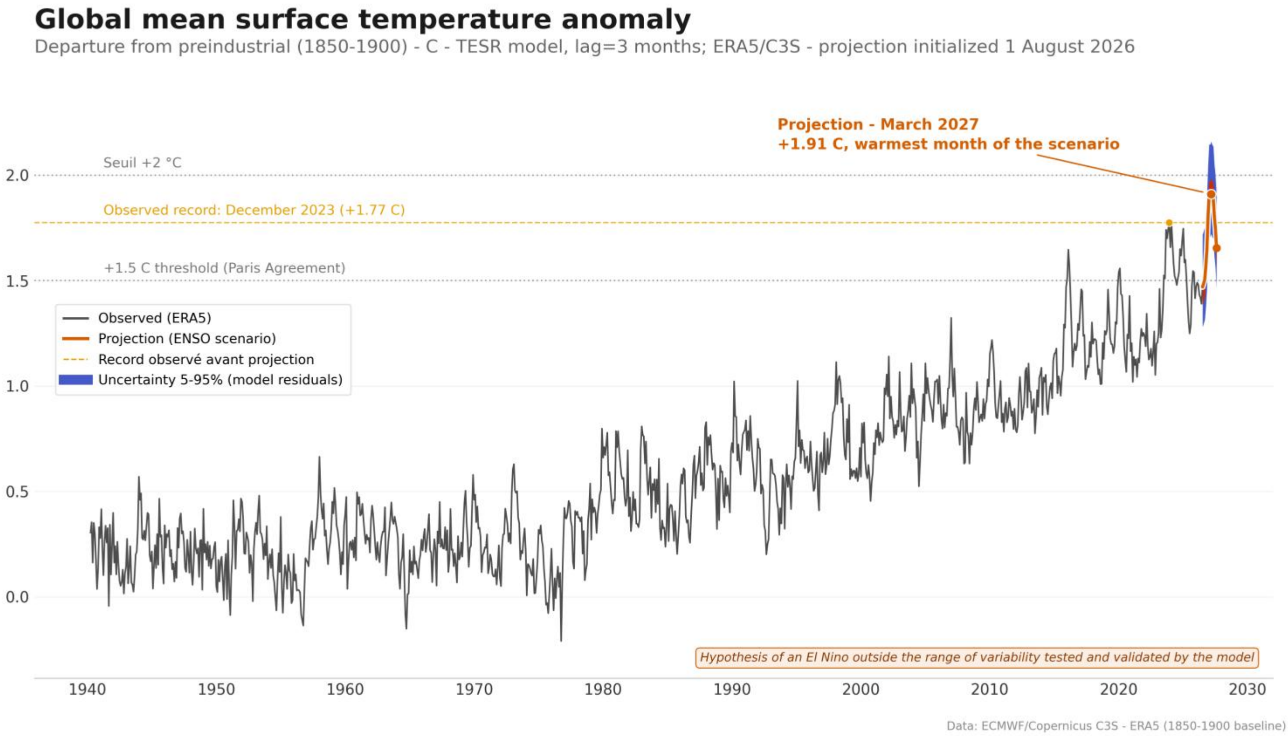

Figure 8. Overview 1940-2030: ERA5 observations and the 2026/2027 central scenario projection from the TESR model, with a 5-95 % uncertainty band based on residuals. The scenario's peak (+1.91 °C) is reached in March 2027, the warmest month of the projected period. Projection initialized on 1 August 2026. Data: ECMWF/Copernicus C3S @ ERA5.

Starting from this initial condition, the central scenario projects a rapid increase in GMSTA from +1.47 °C in July to +1.90 °C in December 2026, followed by a broad plateau between +1.89 °C and +1.91 °C from December 2026 to May 2027, before a gradual decline to +1.66 °C in August 2027 (Fig. 8). The maximum occurs in March 2027, at +1.91 °C. This timing is consistent with the November 2026 peak in the prescribed ONI scenario (Figs. 6 and 9), with the three-month separation corresponding to the optimal lag (τ=3 months) identified during model calibration.

https://doi.org/10.5194/egusphere-2026-5348
Preprint. Discussion started: 7 September 2026

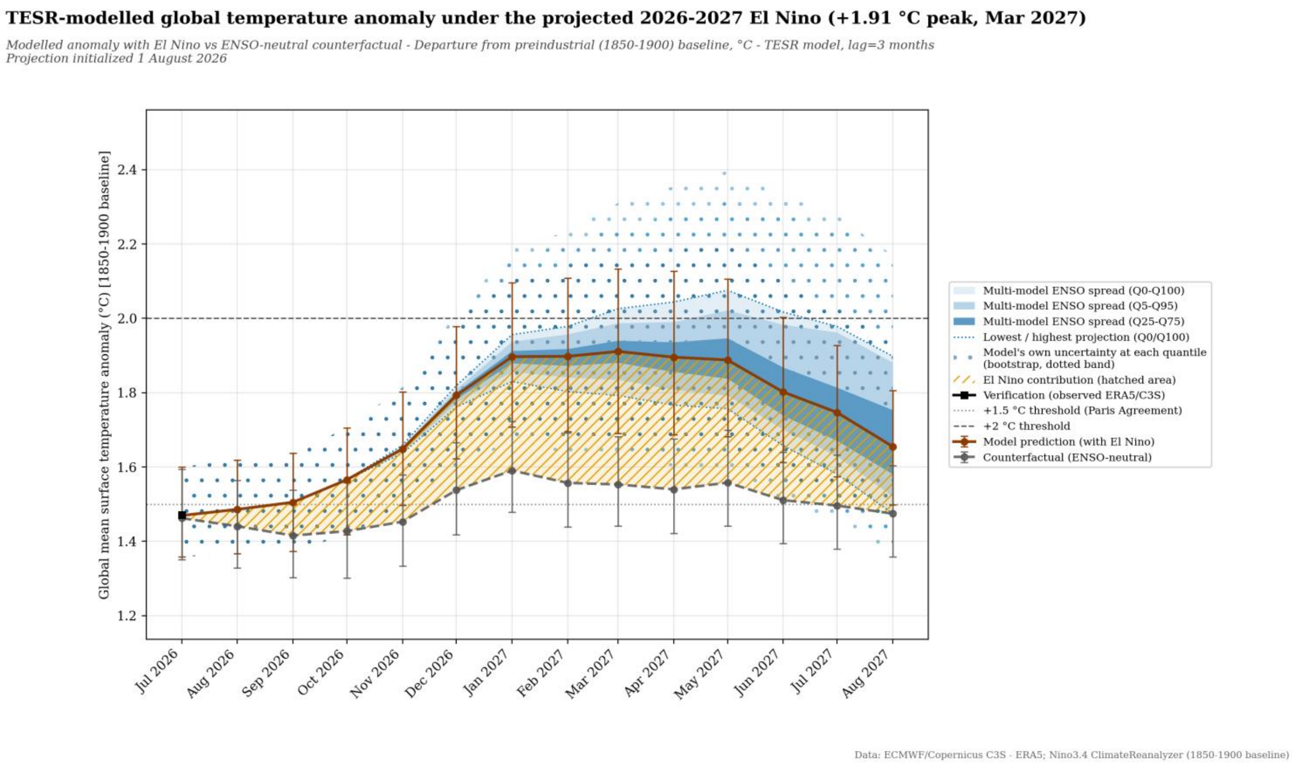

Figure 9. Detailed monthly projection of the GMSTA anomaly, initialized on 1 August 2026, with July 2026 shown as the last observed month, covering July 2026–August 2027: central scenario with El Niño vs. counterfactual neutral ENSO, multi-model dispersion of the ENSO scenario (Q0–Q100, Q5–Q95, Q25–Q75) and model-specific uncertainty at each quantile (bootstrap). The hatched area represents the net contribution attributable to El Niño. Data: ECMWF/Copernicus C3S @ ERA5; Niño3.4 ClimateReanalyzer.

TESR projects a progressive increase in GMSTA through late 2026 and early 2027, reaching a maximum central anomaly of approximately +1.91 °C in March 2027 before gradually declining through August 2027. To provide a fully traceable record of the prospective experiment, Table 6 reports the month-by-month TESR projections from July 2026 to August 2027, based on the model initialized on 1 August 2026. The table reports the central GMSTA estimate and its uncertainty interval, together with the decomposition into the background trend, seasonal component, ENSO contribution and ENSO-neutral counterfactual. These values correspond to the prospective model output and were not subsequently adjusted using observations from the forecast period.

https://doi.org/10.5194/egusphere-2026-5348
Preprint. Discussion started: 7 September 2026

Detailed monthly table - 2026-2027 (projection)

TESR model - exact linear decomposition; ENSO = Model - Counterfactual (= Trend + Seasonal); Seasonal isolated separately from the Counterfactual to assess its own share; verification = ERA5/C3S observation (1/14 mois observés, réf. 1850-1900)
90% CI by moving-block bootstrap (n=300, Kunsch 1989) on all columns except Verification (fixed observation); CI of the External variability derived by symmetry of the Model's (sign reversed)
†: |%| > 100 -- Trend+Seasonal+ENSO=Total is exact in °C, but an individual % can exceed 100 (or be negative) when another component has a sign opposite to the Total (often the Seasonal term); trust the °C value in that case, not the %
Official scenario, initialized 1 August 2026

Month	Model (°C)	Trend (°C | %)	Seasonal (°C | %)	Counterfactual (trend+seasonal, °C)	ENSO (°C | %)	Verification (°C)	External variability (°C | %)
Jul 2026	+1.47 °C [+1.36;+1.60] °C	+1.57 °C [+1.46;+1.70] °C +107%† [+105;+110]%	-0.11 °C [-0.14;-0.08] °C -8% [-10;-5]%	+1.46 °C [+1.35;+1.59] °C	+0.01 °C [+0.00;+0.01] °C +0% [+0;+1]%	+1.47	+0.00 °C [-0.13;+0.11] °C +0% [-9;+8]%
Aug 2026	+1.49 °C [+1.37;+1.62] °C	+1.58 °C [+1.47;+1.71] °C +106%† [+103;+109]%	-0.14 °C [-0.17;-0.11] °C -9% [-11;-7]%	+1.44 °C [+1.33;+1.56] °C	+0.05 °C [+0.03;+0.07] °C +3% [+2;+5]%	—	—
Sep 2026	+1.51 °C [+1.37;+1.64] °C	+1.58 °C [+1.47;+1.71] °C +105%† [+101;+109]%	-0.16 °C [-0.19;-0.13] °C -11% [-13;-9]%	+1.42 °C [+1.30;+1.54] °C	+0.09 °C [+0.05;+0.13] °C +6% [+3;+9]%	—	—
Oct 2026	+1.57 °C [+1.42;+1.71] °C	+1.58 °C [+1.47;+1.71] °C +101%† [+96;+106]%	-0.15 °C [-0.18;-0.12] °C -10% [-12;-8]%	+1.43 °C [+1.30;+1.56] °C	+0.14 °C [+0.08;+0.21] °C +9% [+5;+13]%	—	—
Nov 2026	+1.65 °C [+1.50;+1.80] °C	+1.58 °C [+1.47;+1.72] °C +96% [+91;+102]%	-0.13 °C [-0.16;-0.11] °C -8% [-10;-6]%	+1.45 °C [+1.33;+1.58] °C	+0.20 °C [+0.11;+0.29] °C +12% [+7;+17]%	—	—
Dec 2026	+1.79 °C [+1.62;+1.98] °C	+1.59 °C [+1.48;+1.72] °C +89% [+83;+94]%	-0.05 °C [-0.07;-0.03] °C -3% [-4;-1]%	+1.54 °C [+1.42;+1.67] °C	+0.26 °C [+0.14;+0.38] °C +14% [+8;+20]%	—	—
Jan 2027	+1.90 °C [+1.71;+2.10] °C	+1.59 °C [+1.48;+1.72] °C +84% [+77;+90]%	+0.00 °C [+0.00;+0.00] °C +0% [+0;+0]%	+1.59 °C [+1.48;+1.72] °C	+0.31 °C [+0.17;+0.46] °C +16% [+10;+23]%	—	—
Feb 2027	+1.90 °C [+1.70;+2.11] °C	+1.59 °C [+1.48;+1.73] °C +84% [+77;+91]%	-0.04 °C [-0.06;-0.01] °C -2% [-3;-1]%	+1.56 °C [+1.44;+1.69] °C	+0.34 °C [+0.19;+0.51] °C +18% [+11;+25]%	—	—
Mar 2027	+1.91 °C [+1.69;+2.13] °C	+1.60 °C [+1.48;+1.73] °C +84% [+76;+91]%	-0.04 °C [-0.07;-0.02] °C -2% [-4;-1]%	+1.55 °C [+1.44;+1.68] °C	+0.36 °C [+0.20;+0.53] °C +19% [+11;+26]%	—	—
Apr 2027	+1.90 °C [+1.69;+2.13] °C	+1.60 °C [+1.49;+1.73] °C +84% [+77;+92]%	-0.06 °C [-0.09;-0.03] °C -3% [-5;-2]%	+1.54 °C [+1.42;+1.68] °C	+0.36 °C [+0.20;+0.53] °C +19% [+11;+26]%	—	—
May 2027	+1.89 °C [+1.68;+2.11] °C	+1.60 °C [+1.49;+1.74] °C +85% [+78;+93]%	-0.04 °C [-0.08;-0.01] °C -2% [-4;-1]%	+1.56 °C [+1.44;+1.70] °C	+0.33 °C [+0.19;+0.49] °C +17% [+10;+24]%	—	—
Jun 2027	+1.80 °C [+1.61;+2.00] °C	+1.60 °C [+1.49;+1.74] °C +89% [+82;+96]%	-0.09 °C [-0.13;-0.06] °C -5% [-7;-3]%	+1.51 °C [+1.39;+1.64] °C	+0.29 °C [+0.16;+0.43] °C +16% [+10;+23]%	—	—
Jul 2027	+1.75 °C [+1.57;+1.93] °C	+1.61 °C [+1.49;+1.74] °C +92% [+86;+99]%	-0.11 °C [-0.14;-0.08] °C -6% [-8;-5]%	+1.50 °C [+1.38;+1.63] °C	+0.25 °C [+0.14;+0.37] °C +14% [+8;+20]%	—	—
Aug 2027	+1.66 °C [+1.50;+1.81] °C	+1.61 °C [+1.49;+1.75] °C +97% [+92;+103]%	-0.14 °C [-0.17;-0.11] °C -8% [-10;-6]%	+1.47 °C [+1.36;+1.60] °C	+0.18 °C [+0.10;+0.27] °C +11% [+6;+16]%	—	—

Data: ECMWF/Copernicus C3S - ERA5; Nino3.4 ClimateReanalyzer (ref. 1850-1900)

Table 6. Summary of the estimated influence of the anthropogenic trend, ENSO, and seasonal residuals on the projected GMSTA trend between July 2026 and August 2027, along with the 90 % Confidence Interval (C.I.) modeled using bootstrapping and the proportion of deterministic variability not explained by the model. Projection initialized on 1 August 2026.

TESR estimates a net ENSO contribution of approximately +0.30 to +0.35 °C between December 2026 and May 2027, defined as the difference between the factual projection and the ENSO-neutral counterfactual (Fig. 9). Over the same period, the counterfactual remains near +1.55 to +1.59 °C, indicating that the modelled background component alone would already exceed +1.5 °C relative to 1850–1900. El Niño therefore acts primarily as an additional amplification of an already elevated background temperature state, rather than being the sole driver of the projected threshold exceedance (Table 6).

4.3.3 Probabilities of threshold exceedance

The exceedance probabilities, calculated using the combined procedure described in Sect. 3.4 (n = 20,000 simulations per month, statistical model uncertainty + multi-model dispersion of the ENSO scenario), is consistent with the results summarized in the introduction to the manuscript: in the peak month (March 2027), exceeding the +1.5 °C threshold is virtually certain (100 %), while exceeding the +2.0 °C threshold reaches 23 to 24 % depending on the interpretation method used (Fig. 10: direct reading from the 20,000 combined draws, 24 %; Fig. 11: reading from the empirical survival function, 23 %). These probabilities reflect the propagated uncertainty of the empirical multi-model ENSO scenario and TESR residuals; they should not be interpreted as frequencies derived from 20,000 independent forecasts.

https://doi.org/10.5194/egusphere-2026-5348
Preprint. Discussion started: 7 September 2026

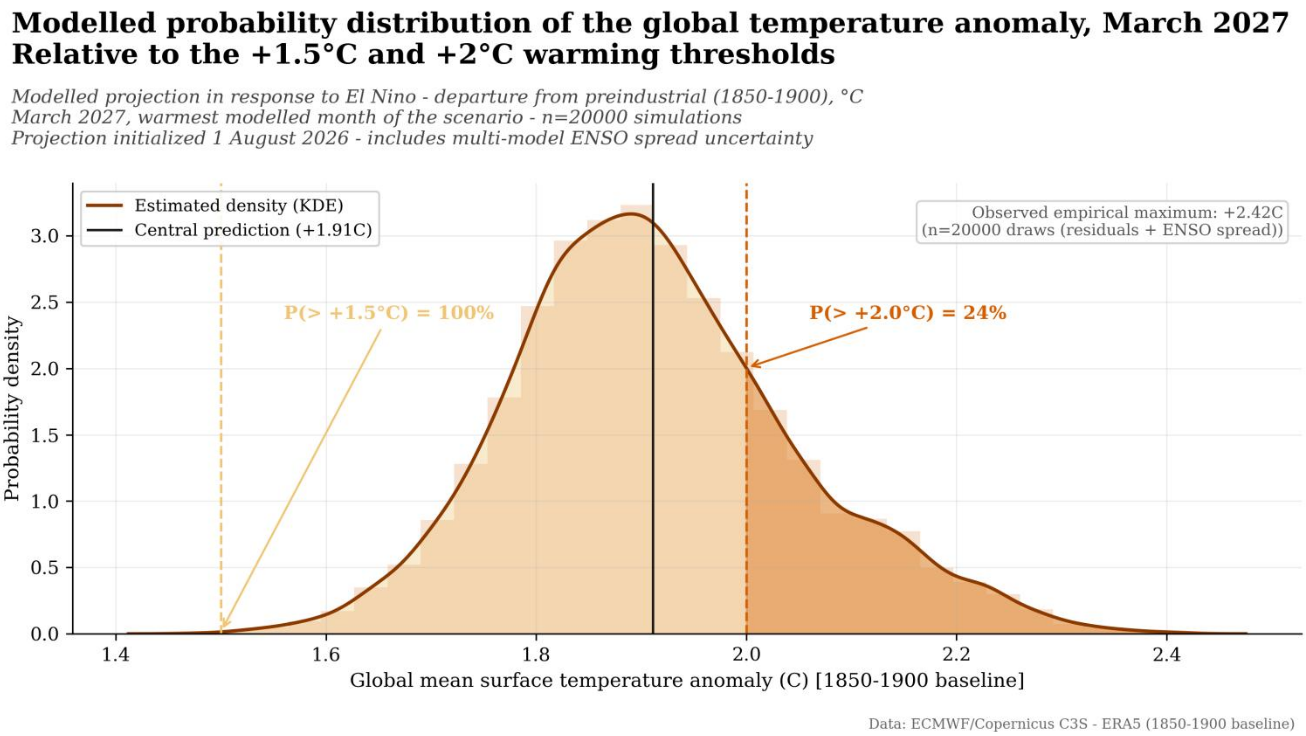

Figure 10. Combined probability density (model residuals + ENSO multi-model dispersion, n = 20,000 runs) of the GMSTA anomaly in March 2027, the warmest month in the scenario. Central prediction: +1.91 °C, initialized on August 1, 2026. Empirical maximum observed across the simulations: +2.44 °C. Data: ECMWF/Copernicus C3S @ ERA5.

The comparison with the counterfactual neutral ENSO scenario (Fig. 11) precisely quantifies the increase in risk attributable to the current El Niño episode: at the +1.5 °C threshold, the probability of exceeding the threshold rises from 64 % (counterfactual world, neutral ENSO) to 100 % (with El Niño), representing a multiplicative factor of approximately ×1.6; at the +2.0 °C threshold, the probability of exceeding the threshold is virtually zero without El Niño (0 %) compared to 23 % with it, indicating that the risk of exceeding this second threshold at this time horizon is almost entirely attributable to the ongoing ENSO episode rather than to the underlying trend alone. The cumulative area between the two survival functions over the interval [1.5 °C; 2.0 °C] is approximately 31 percentage- °C points, a summary measure of the cumulative excess risk attributable to El Niño across the entire range of intermediate thresholds between the two benchmarks of the Paris Agreement.

https://doi.org/10.5194/egusphere-2026-5348
Preprint. Discussion started: 7 September 2026

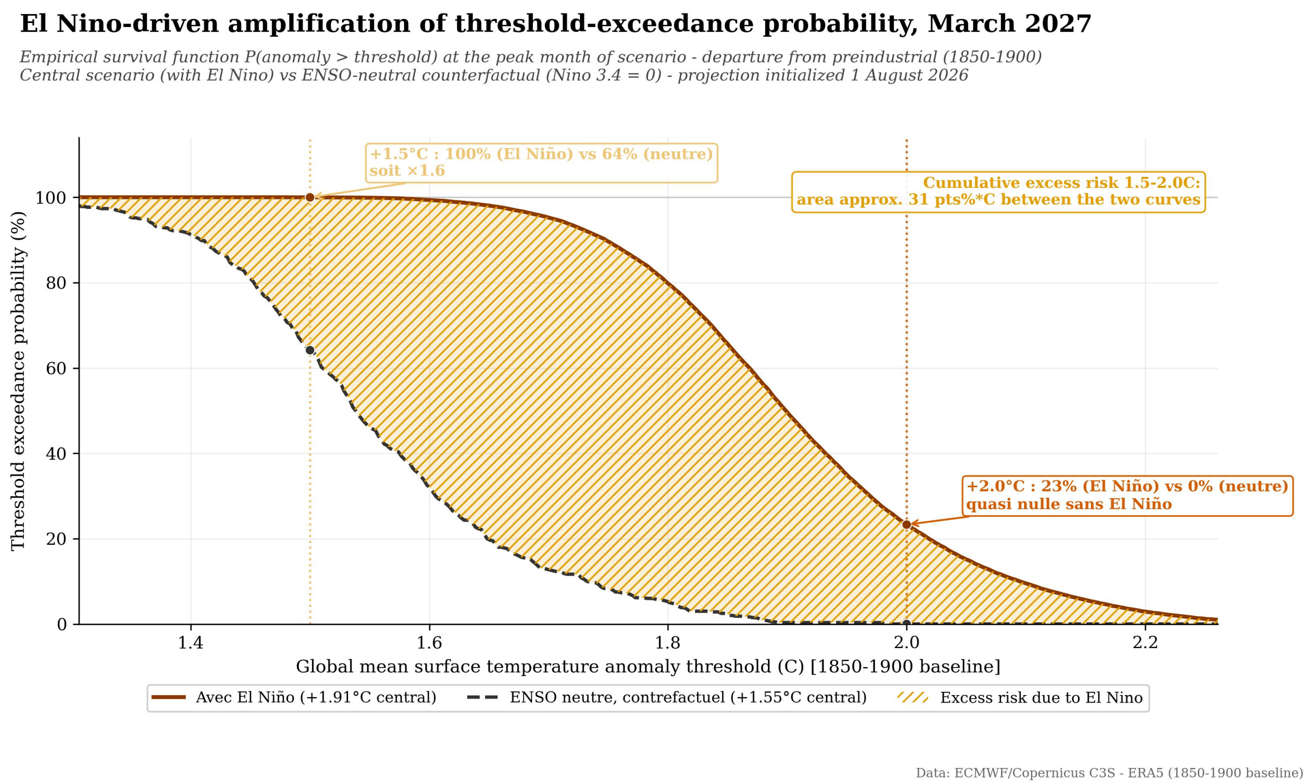

Figure 11. Empirical survival function P(anomaly > threshold) in the scenario's peak month (March 2027): central scenario (with El Niño) vs. counterfactual neutral ENSO. Projection initialized on 1 August 2026. The hatched area represents the excess risk of exceedance attributable to El Niño. Data: ECMWF/Copernicus C3S @ ERA5.

When viewed in the context of recent climate trends rather than solely against the preindustrial baseline, the projected central anomaly for March 2027 (+1.91 °C) lies 3.0 standard deviations above the average of the monthly anomalies observed over the 2016–2026 decade (adjusted normal distribution, $\mu = +1.32$ °C, $\sigma = 0.20$ °C; Fig. 12), which is approximately the 100th percentile of this recent historical distribution. Taken in isolation, this finding illustrates not so much an extreme statistical anomaly in the broad sense (the model specifically anticipates an El Niño episode that is itself exceptional) as a direct and expected consequence of the combination of a persistent background warming component and an exceptional ENSO episode, consistent with the attribution decomposition developed below (Sect. 4.5).

https://doi.org/10.5194/egusphere-2026-5348
Preprint. Discussion started: 7 September 2026

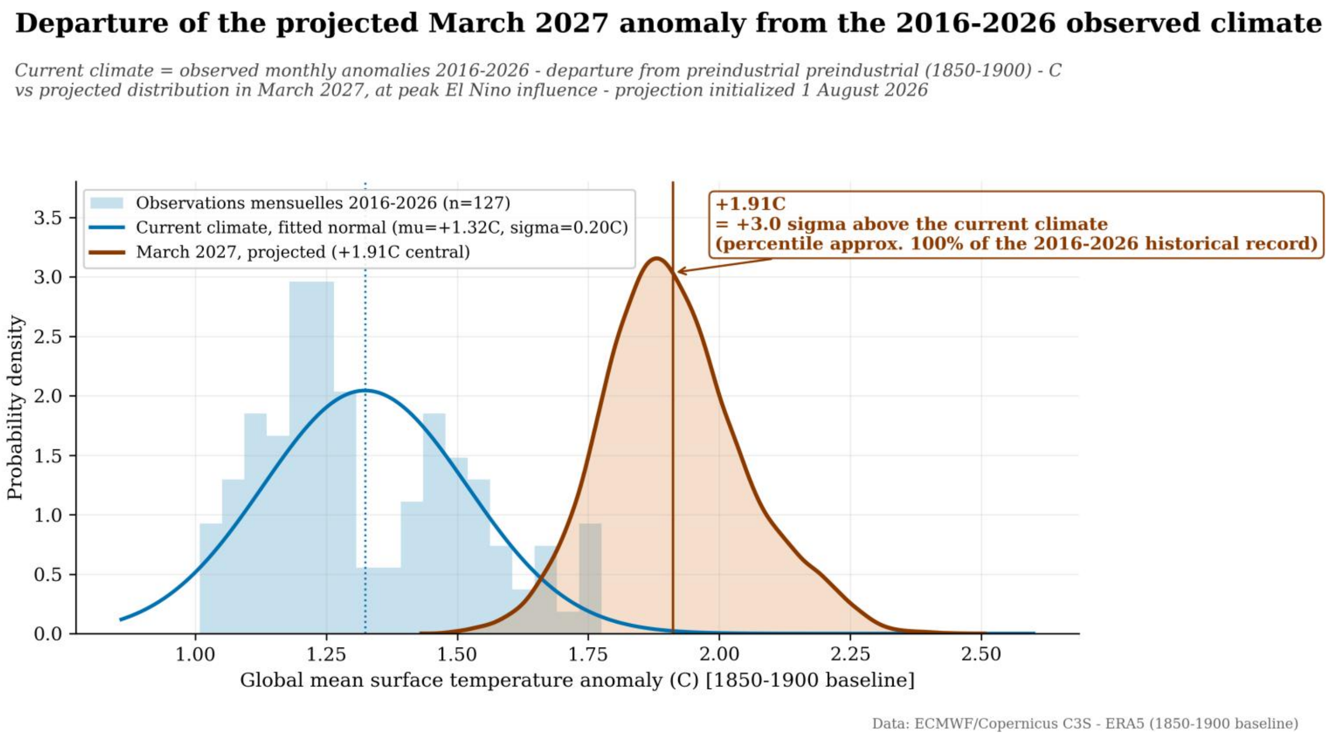

Figure 12. Comparison of the distribution projected for March 2027 (under El Niño conditions) with the distribution of observed monthly anomalies over the "current climate" decade of 2016–2026 (n = 127 months). Data: ECMWF/Copernicus C3S @ ERA5.

https://doi.org/10.5194/egusphere-2026-5348
Preprint. Discussion started: 7 September 2026

Fig. 13 summarizes the corresponding month-by-month probabilities of exceeding selected global warming thresholds. The probability of exceeding +1.5 °C increases rapidly during late 2026 and reaches 100 % from January 2027 onward in the central prospective scenario. The probability of exceeding +2.0 °C becomes non-negligible from December 2026, reaches 23 % in March 2027, and remains at 23 % in May 2027 before declining thereafter.

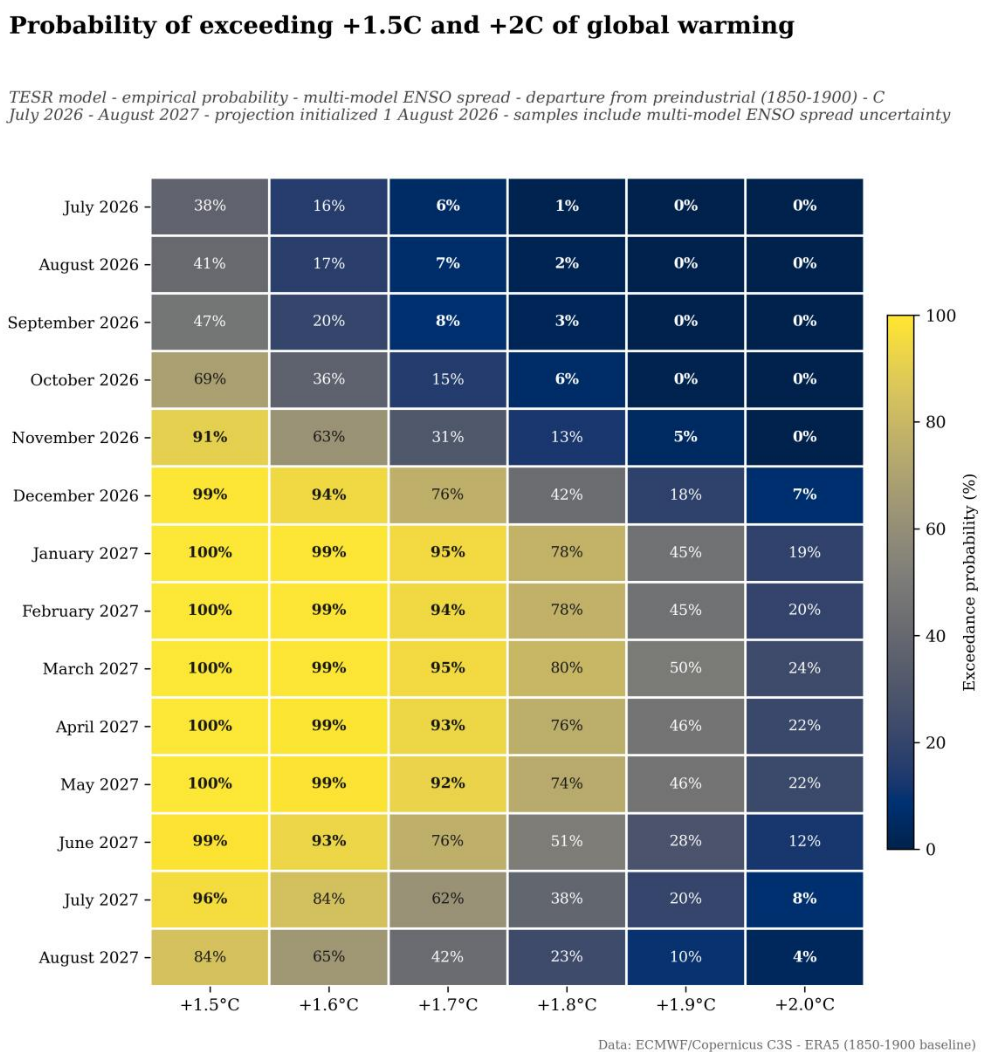

Figure 13. Month-by-month probabilities of exceeding selected global mean surface temperature anomaly thresholds from July 2026 to August 2027 under the prospective 2026–2027 ENSO scenario. Probabilities are derived from the TESR predictive distributions using the model configuration initialized on 1 August 2026. The heatmap shows the probability of exceeding +1.5 °C and +2.0 °C relative to the 1850–1900 reference period for each month. Values represent the prospective model output and were not subsequently adjusted using observations from the forecast period.

https://doi.org/10.5194/egusphere-2026-5348
Preprint. Discussion started: 7 September 2026

These probabilities quantify the transient threshold risk associated with the specified 2026–2027 ENSO scenario and should not be interpreted as evidence of a sustained exceedance of the corresponding Paris Agreement warming levels.

4.3.4 Sensitivity analysis of the +2.0 °C exceedance probability

A sensitivity analysis of the prospective exceedance probabilities was used to investigate the systematic underestimation of the highest historical GMSTA peaks found in Sect. 4.2. The analysis was limited to March 2027, the scenario's peak month, when the probability of exceeding +2.0 °C is highest and the central TESR projection reaches +1.91 °C. Additive corrections were only applied as a sensitivity experiment to the simulated March 2027 GMSTA distribution, leaving the central probabilistic forecast unaltered.

The observed peak underestimation varied from +0.145 °C to +0.224 °C, with a mean of +0.174 °C, over the course of the three historical very strong El Niño episodes. The probability of exceeding +2.0 °C is significantly increased when these values are applied as additive perturbations to the simulated distribution (Fig. 14, Table 7). The exceedance probability, uncorrected, is 23.7 %. This probability is raised to about 45.19 % by applying a +0.145 °C correction, which corresponds to the lower end of the empirically observed range. It is further increased to about 51.5 % when the mean historical bias of +0.174 °C is used, whereas the correction of +0.224 °C, which corresponds to the largest observed historical underestimation, yields about 59.76 %.

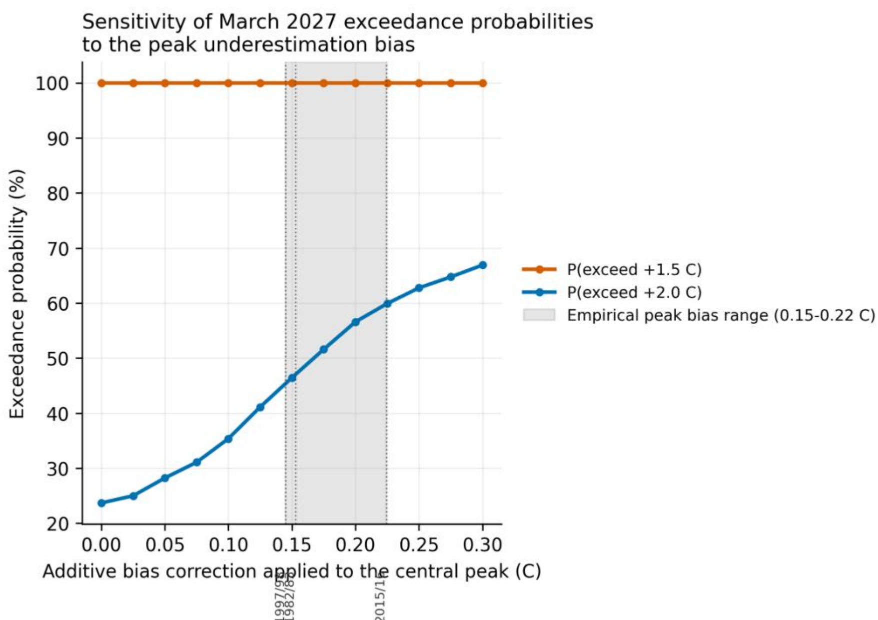

Figure 14. Sensitivity of the March 2027 probability of exceeding +2.0 °C to additive corrections for the historical peak

underestimation bias. The uncorrected probability is 23.70 %. Additive corrections of +0.145, +0.174, and +0.224 °C, corresponding respectively to the minimum, mean, and maximum empirical peak underestimation identified in the historical calibration episodes, increase the exceedance probability to 45.19 %, 51.50 %, and 59.76 %.

Bias correction (°C)	Corrected central peak (°C)	*P > 1.5* °C	*P > 2.0* °C
0.000	1.911	99.975	23.695
0.025	1.936	99.975	25
0.050	1.961	99.975	28.23
0.075	1.986	99.975	31.085
0.100	2.011	99.975	35.38
0.125	2.036	99.975	41.12
0.150	2.061	99.975	46.45
0.175	2.086	99.975	51.595
0.200	2.111	99.975	56.584
0.225	2.136	99.975	59.915
0.250	2.161	99.975	62.755
0.275	2.186	99.975	64.75
0.300	2.211	99.975	66.9

Table 7. Corresponding raw values in support of Fig. 14 for March 2027.

The estimated probability of exceeding +2.0 °C thus rises from 23.7 % to 45.19-59.76 % over the entire empirically supported range of +0.145 to +0.224 °C. In comparison to the uncorrected estimate, this represents an increase of 21.49-36.06 percentage points, or a factor of 1.9 to 2.5. In contrast, since almost all simulated outcomes in the central scenario already exceed the threshold, the probability of exceeding +1.5 °C stays saturated at 100 % throughout this sensitivity range.

https://doi.org/10.5194/egusphere-2026-5348
Preprint. Discussion started: 7 September 2026

As a result, the sensitivity is almost entirely focused on the rarer +2.0 °C threshold, where the exceedance probability is significantly altered by a relatively small shift in the upper portion of the simulated distribution. Because only three historical peak episodes are used to infer the magnitude of the correction, these results do not represent a bias-corrected forecast. Instead, they measure how much the prospective +2.0 °C probability is dependent on the unresolved peak-amplitude bias found in the retrospective analysis. As a result, Sect. 4.3.3 is kept as the uncorrected model estimate, and the sensitivity range offers an empirically based indicator of the related structural uncertainty.

4.3.5 Semester and Annual Averages

In addition to the monthly breakdown (Table 6), three higher-level averages provide an annual perspective on the scenario:

First half of 2027 (January-June). The average GMSTA anomaly projected for this period, which includes the scenario's peak (March 2027), is +1.88 °C [90 % confidence interval for monthly averages: +1.80; +1.91] °C, which is already +0.38 °C above the Paris Agreement threshold.

Year 2026 (projection). By combining the first six observed months (ERA5, +1.39 to +1.49 °C depending on the month) and the last six months projected by the model (Table 6, +1.47 to +1.79 °C), the average GMSTA anomaly for the full year 2026 would be +1.51 °C [90 % confidence interval: +1.44; +1.59] °C, making 2026 the second-hottest year on record, behind 2024 (+1.60 °C). In a more extreme scenario, and given the model's systematic underestimation as the climate system's response to El Niño approaches its peak, the annual anomaly for 2026 could exceed +1.60 °C above pre-industrial levels, making this year the hottest on record since reliable measurements began in the 20th century.

Year 2027 (extended projection, see Sect. 4.4.1). According to the scenario chosen for the ENSO transition in the second half of 2027 (H2 2027), the 2027 annual average would range between +1.73 °C (the "strong La Niña" scenario) and +1.76 °C (the "neutral ENSO" scenario), with the central scenario ("moderate La Niña") yielding +1.75 °C. This low sensitivity of the annual average to the ENSO scenario for the second half of the year (a difference of only 0.03 °C among the three scenarios) is explained by the dominant weight of the first half of the year (H1 2027), which is directly influenced by the peak of El Niño, in the annual average.

Period	$\overline{\text{GMSTA}}$	Type
H1 2027 (January-June)	+1.88 °C [+1.80 ; +1.91] °C	C3S multi-model projection (Start date: 1 August 2026)
2026	+1.51 °C [+1.44 ;	Observed (January-July) + Projected (August-December)

https://doi.org/10.5194/egusphere-2026-5348
Preprint. Discussion started: 7 September 2026

	+1.59] °C	
2027 (Strong La Niña)	+1.73 °C [+1.57 ; +1.89] °C	Extended H2 2027 (author assumption)
2027 (Moderate La Niña)	+1.75 °C [+1.59 ; +1.91] °C	Extended H2 2027 (author assumption)
2027 (Neutral ENSO)	+1.76 °C [+1.59 ; +1.92] °C	Extended H2 2027 (author assumption)

Table 8. Half-yearly and annual averages derived from Table 6 (H1 2027, year 2026) and from the extension described in Sect. 4.4.1 (the whole of year 2027)

4.4 Exploratory extension beyond the official ENSO forecast horizon

4.4.1 Extended full-year 2027 hypothesis

The official multi-model scenario (Sect. 4.3.1, Figs. 6-7) only covers the ONI/Niño 3.4 index up to April 2027 (the last available data point in the Climate Dashboard envelope initialised on 1 August 2026), with the GMSTA being derived from this up to August 2027. To provide a complete picture of the year 2027, the second half of the year (July-December) is extended here under an explicit ENSO transition assumption, which is distinct in nature from the rest of the manuscript: this is no longer an aggregated multi-model scenario, but an author-constructed hypothesis based on historical analogy, informed by the observed trajectory of the Niño 3.4 index following the peak of each of the three reference episodes (1982/83, 1997/98, 2015/2016, see Sect. 4.3.1), for which the shift towards a La Niña phase, of varying intensity, is a common feature of the major El Niño episodes during the observational period.

Three trajectories are selected for the second half of 2027, anchored to the latest official reading (April 2027, +2.30 °C, Fig. 15, Table 9):

Neutral ENSO (lower bound of the decline): the decline slows and stabilises near 0 °C from September 2027, mirroring the mildest transition observed (2016/2017, which produced only a weak La Niña);

Moderate La Niña (central scenario): a steady decline towards a weak to moderate La Niña by the end of the year (-0.6 to -0.7 °C in December 2027);

https://doi.org/10.5194/egusphere-2026-5348
Preprint. Discussion started: 7 September 2026

Strong La Niña (upper limit of decline): a rapid decline crossing the conventional threshold for a strong La Niña (ONI ≤ -1.5 °C) as early as October-November 2027, without exceeding the most extreme values recorded during the period 1950–2026 (the 1973/74 La Niña, ONI ≈ -2.1 °C).

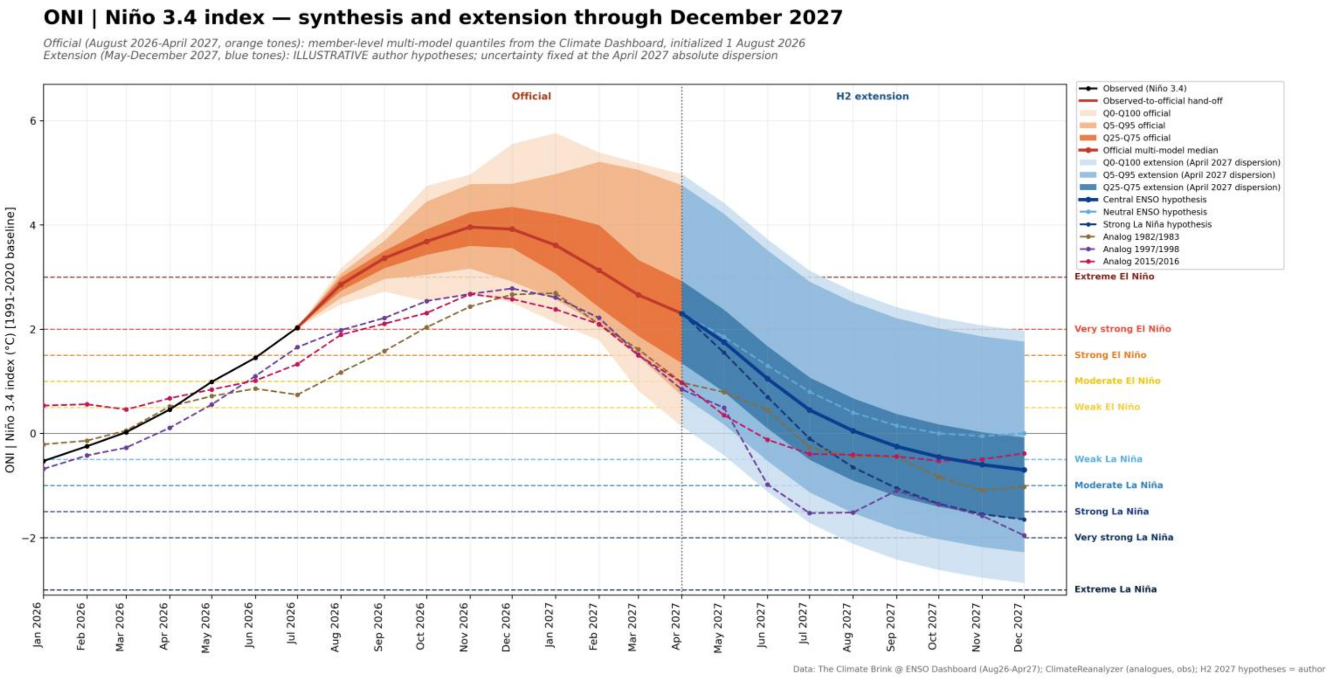

Figure 15. As for Fig. 6 but extended through December 2027 with the three hypotheses cited above.

https://doi.org/10.5194/egusphere-2026-5348
Preprint. Discussion started: 7 September 2026

ONI under the three H2 2027 hypotheses (extension, author scenario)

May-December 2027 - ILLUSTRATIVE author hypotheses (not a multi-model scenario), ONI / Nino 3.4 index, 1991-2020 baseline

Month	Neutral ENSO (ONI, °C)	Central (moderate La Nina) (ONI, °C)	Strong La Nina (ONI, °C)
May 2027	+1.85 °C	+1.75 °C	+1.55 °C
Jun 2027	+1.30 °C	+1.05 °C	+0.70 °C
Jul 2027	+0.80 °C	+0.45 °C	-0.10 °C
Aug 2027	+0.40 °C	+0.05 °C	-0.65 °C
Sep 2027	+0.15 °C	-0.25 °C	-1.05 °C
Oct 2027	+0.00 °C	-0.45 °C	-1.35 °C
Nov 2027	-0.05 °C	-0.60 °C	-1.55 °C
Dec 2027	+0.00 °C	-0.70 °C	-1.65 °C

H2 2027 hypotheses: author

Table 9. Author-defined ONI scenarios for May–December 2027. Monthly Niño 3.4 ONI values under three illustrative hypotheses for the evolution of ENSO from May to December 2027: a neutral scenario, a central scenario, and a strong La Niña scenario. These values represent author-defined sensitivity scenarios and are not official model forecasts. They are intended to assess the sensitivity of projected GMSTA to alternative ENSO evolutions beyond the April 2027 forecast horizon.

These three ENSO trajectories are fed back into the unmodified TESR model (same coefficients, same 3-month causal smoothing, same lag = 3 months). Fig. 16 and Table 10 (below) illustrates the three ENSO trajectories and their translation into GMSTA anomalies.

https://doi.org/10.5194/egusphere-2026-5348
Preprint. Discussion started: 7 September 2026

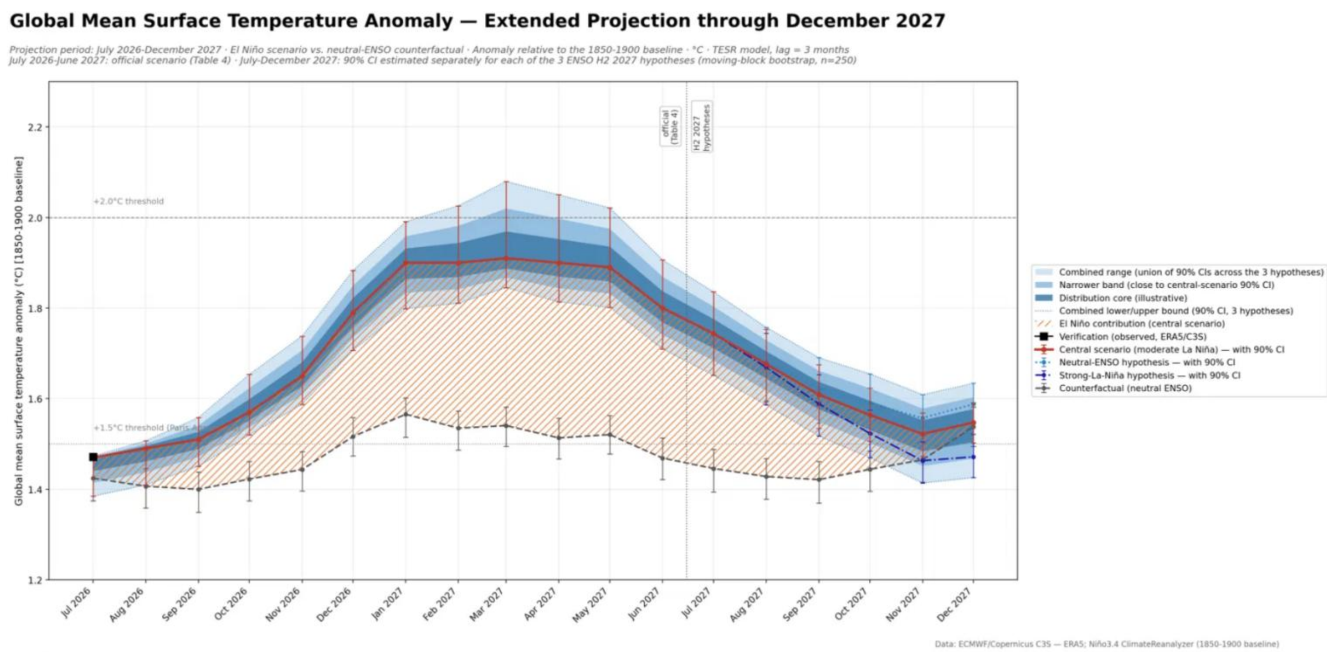

Figure 16. ENSO scenarios for 2026-2027 (Niño 3.4): official multi-model trajectory (August 2026-April 2027, initialized on 1 August 2026) followed by three transition scenarios for May-December 2027 (neutral ENSO / moderate La Niña / strong La Niña) (a), and associated GMSTA anomaly (b). Annual averages for 2027: +1.73 to +1.76 °C depending on the scenario.

https://doi.org/10.5194/egusphere-2026-5348
Preprint. Discussion started: 7 September 2026

Monthly GMSTA decomposition under the three H2 2027 ENSO hypotheses

September-December 2027 extension (author hypotheses), spliced onto the official scenario at August 2027 - TESR model, exact linear decomposition:
ENSO = Model - Counterfactual (= Trend + Seasonal) - departure from preindustrial baseline (1850-1900), °C
90% CI by moving-block bootstrap (n=250) on Model and Counterfactual only; Trend/Seasonal/ENSO shown as point estimates
†: |%| > 100 -- Trend+Seasonal+ENSO=Model is exact in °C, but an individual % can exceed 100 (or be negative) when another component has a sign opposite to the Model; trust the °C value

a) Neutral ENSO hypothesis

Month	Model (°C)	Trend (°C | %)	Seasonal (°C | %)	Counterfactual (trend+seasonal, °C)	ENSO (°C | %)
Sep 2027	+1.60 °C [+1.50;+1.65] °C	+1.55 °C +97%	-0.15 °C -10%	+1.40 °C [+1.36;+1.45] °C	+0.20 °C +13%
Oct 2027	+1.57 °C [+1.47;+1.61] °C	+1.55 °C +99%	-0.13 °C -9%	+1.42 °C [+1.37;+1.46] °C	+0.15 °C +9%
Nov 2027	+1.53 °C [+1.47;+1.57] °C	+1.56 °C +102%†	-0.12 °C -8%	+1.44 °C [+1.40;+1.49] °C	+0.09 °C +6%
Dec 2027	+1.56 °C [+1.52;+1.62] °C	+1.56 °C +100%	-0.05 °C -3%	+1.51 °C [+1.48;+1.57] °C	+0.05 °C +3%

b) Central hypothesis (moderate La Niña)

Month	Model (°C)	Trend (°C | %)	Seasonal (°C | %)	Counterfactual (trend+seasonal, °C)	ENSO (°C | %)
Sep 2027	+1.59 °C [+1.50;+1.64] °C	+1.56 °C +98%	-0.15 °C -10%	+1.40 °C [+1.36;+1.45] °C	+0.19 °C +12%
Oct 2027	+1.54 °C [+1.47;+1.58] °C	+1.56 °C +101%†	-0.13 °C -9%	+1.42 °C [+1.37;+1.47] °C	+0.12 °C +8%
Nov 2027	+1.50 °C [+1.45;+1.55] °C	+1.56 °C +104%†	-0.12 °C -8%	+1.44 °C [+1.40;+1.49] °C	+0.06 °C +4%
Dec 2027	+1.53 °C [+1.49;+1.58] °C	+1.56 °C +102%†	-0.05 °C -3%	+1.52 °C [+1.49;+1.57] °C	+0.01 °C +1%

c) Strong La Niña hypothesis

Month	Model (°C)	Trend (°C | %)	Seasonal (°C | %)	Counterfactual (trend+seasonal, °C)	ENSO (°C | %)
Sep 2027	+1.58 °C [+1.49;+1.62] °C	+1.56 °C +99%	-0.15 °C -10%	+1.41 °C [+1.37;+1.46] °C	+0.17 °C +11%
Oct 2027	+1.51 °C [+1.44;+1.55] °C	+1.57 °C +104%†	-0.13 °C -9%	+1.43 °C [+1.38;+1.47] °C	+0.08 °C +5%
Nov 2027	+1.45 °C [+1.40;+1.50] °C	+1.57 °C +108%†	-0.12 °C -8%	+1.45 °C [+1.41;+1.50] °C	-0.00 °C -0%
Dec 2027	+1.46 °C [+1.44;+1.53] °C	+1.57 °C +108%†	-0.05 °C -3%	+1.53 °C [+1.49;+1.58] °C	-0.07 °C -5%

Data: ECMWF/Copernicus C3S — ERA5; Nino3.4 ClimateReanalyzer (1850-1900 climatology)

Table 10. Monthly GMSTA decomposition under three illustrative ENSO hypotheses for September–December 2027. Monthly GMSTA estimates and 90 % confidence intervals under three author-defined ENSO hypotheses: a) neutral ENSO, b) moderate La Niña (central), and c) strong La Niña. The decomposition separates the modelled background warming trend, seasonal component, and net ENSO contribution, with the counterfactual corresponding to the trend plus seasonal components in the absence of ENSO forcing. Confidence intervals are estimated using a moving-block bootstrap with 250 replicates for the Model and Counterfactual components; the Trend, Seasonal, and ENSO contributions are reported as point estimates. The H2 2027 ENSO trajectories are illustrative author-defined hypotheses and are not official ENSO forecasts. Percentages are expressed relative to the corresponding Model value and may exceed 100 % when another component has an opposite sign.

Under all three scenarios, the GMSTA anomaly at the end of 2027 (December) would return to between +1.47 and +1.59 °C, a level that would remain close to or slightly above the +1.5 °C threshold regardless of the rate of ENSO transition chosen, which illustrates that, once the peak influence of El Niño has passed, the GMSTA anomaly converges fairly rapidly towards

https://doi.org/10.5194/egusphere-2026-5348
Preprint. Discussion started: 7 September 2026

a regime once again dominated solely by the long-term trend, in contrast to the winter peak of 2026/2027, where the net contribution of El Niño remains substantial (Sect. 4.5).

This extension is based on an assumption derived from historical analogy rather than on a validated multi-model scenario: it is of an exploratory and illustrative nature, falling outside the walk-forward probabilistic framework on which the rest of the manuscript is based (Sect 3.7.1).

4.5 Decomposition of the share of variability responsible for the modelled rise in global temperatures

The factual/counterfactual decomposition applied to the 2026/2027 scenario makes it possible to isolate, for the month when El Niño's influence on GMSTA peaks (April 2027 in the central scenario), a time window comparable to those of the 1982/83 and 1997/98 episodes (April 1983 and April 1998, respectively), the respective contributions of the background warming component, the net ENSO contribution, and the model's seasonal residual (Fig. 17). Within the model, the +1.90 °C total anomaly for this month is decomposed into +1.60 °C [+1.49; +1.74] °C for the modelled background warming component (84 % of the total), +0.36 °C [+0.14; +0.76] °C (min-max range as shown is Fig. 17, to be compared with the 90 % confidence interval of +0.20 to +0.53 °C shown in Table 6) for the net El Niño contribution (19 %) and -0.06 °C for the residual seasonal component of the model (-3 %). The proportion of external variability not explained by the model (model-observation difference, see Tables 2-4) remains unavailable (n.a.) at this stage, due to a lack of observations for a month that was still in the future at the time of writing.

https://doi.org/10.5194/egusphere-2026-5348
Preprint. Discussion started: 7 September 2026

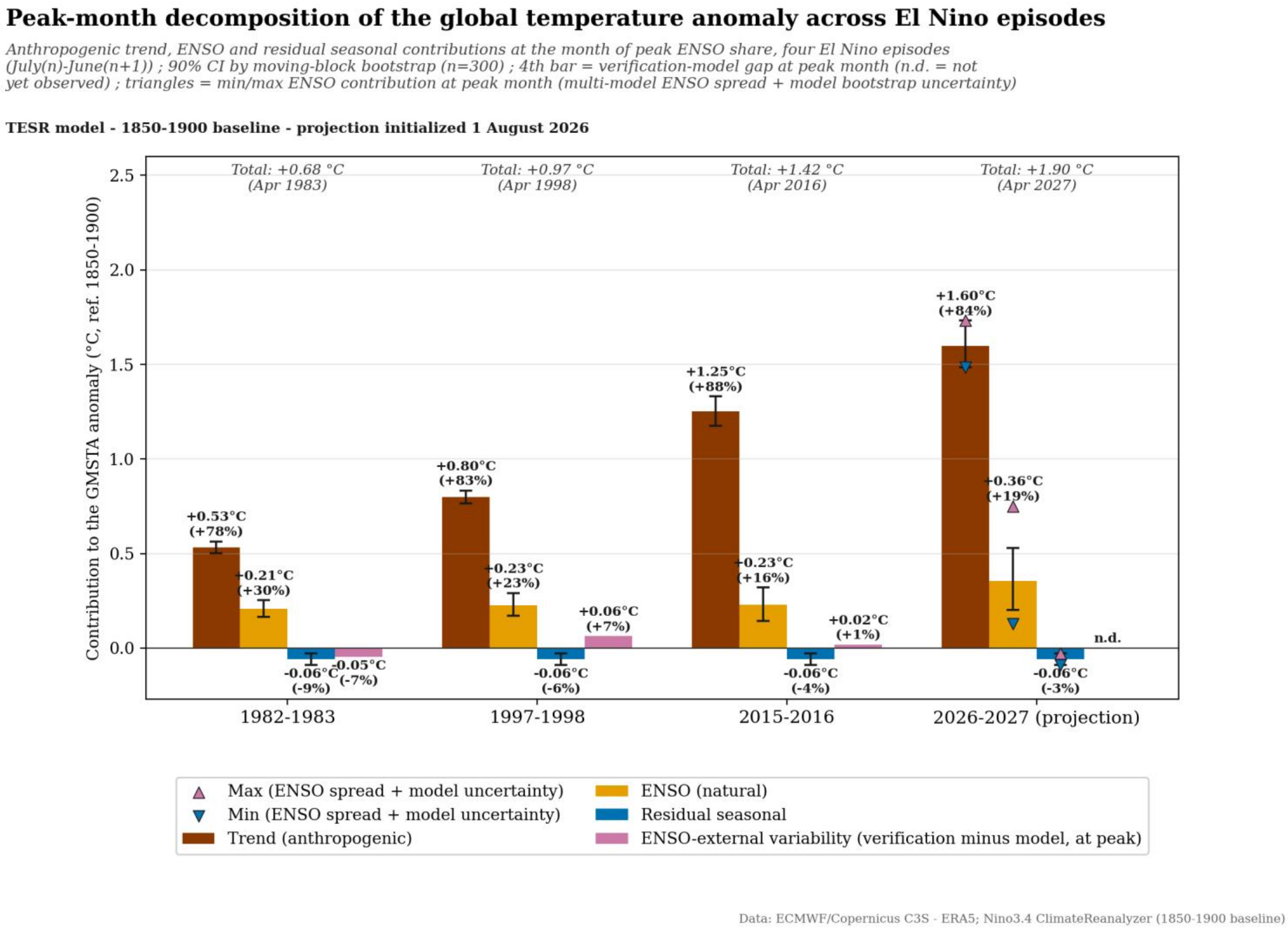

Figure 17. Comparative contribution of the modelled background warming component, El Niño and the seasonal residual to the GMSTA anomaly in the peak month of each of the four episodes studied (1982/83, 1997/98, 2015/2016 and 2026/2027 in the projection). TESR model, 1850-1900 climatology, projection initialised on 1 August 2026. Data: ECMWF/Copernicus C3S @ ERA5; Niño3.4 ClimateReanalyzer.

When considered within the series of the four episodes studied (Table 11, Fig. 17), the net contribution of El Niño to the GMSTA increases monotonically in absolute terms with the peak ONI intensity. This is consistent with the inter-event relationship identified across the three historical episodes, although the 2026/2027 value lies outside the range on which this relationship was empirically evaluated. The relative share of this contribution in the monthly balance, however, does not continue the steady decline observed across the three historical episodes (30 % → 23 % → 16 %): it rises to 19 % in 2026/2027, breaking the trend of relative compression of El Niño's influence already documented in Sect. 4.2. This break can be explained by the unprecedented intensity of the 2026/2027 scenario, in which the projected median ONI is approximately 1.4 times higher than the 2015/2016 record, which partially offsets, in relative terms, the continuous increase

https://doi.org/10.5194/egusphere-2026-5348
Preprint. Discussion started: 7 September 2026

in the modelled anthropogenic warming component, without, however, reaching the relative share observed in 1982/83.

Episode	Peak ONI (°C)	Modelled anthropogenic warming component (°C)	Net ENSO contribution (°C)	Relative ENSO contribution (%)
1982/83	2.2	+0.53	+0.21	30 %
1997/98	2.4	+0.80	+0.23	23 %
2015/16	2.8	+1.25	+0.23	16 %
2026/27	3.96	+1.60	+0.36	19 %

Table 11. Comparative summary of the trend/ENSO decomposition during the month when El Niño's influence on the GMSTA was at its peak for the four episodes studied. Central point estimates; see Figs. 3-5 and Fig. 17 for the 90 % confidence intervals. Projection initialised on 1 August 2026.

This breakdown must be interpreted with the same methodological caveats as those detailed in Sect. 3.10 for the three historical episodes, reinforced here by the forward-looking nature of the scenario and the fact that it lies outside the observed range. The 90 % confidence interval for the net ENSO contribution is substantially wider than for previous episodes (+0.14 to +0.76 °C, compared, for example, with +0.14 to +0.32 °C in 2015/2016), directly reflecting the spread of the multi-model ENSO scenario itself (Sect. 3.4, Multi-model weighting), in addition to uncertainty from the statistical model residuals. Those sources of scenario uncertainty, by definition, were not present for the previously observed episodes.

5 Discussion

A warmer global temperature baseline changes the context in which ENSO-related variability is expressed. While the historical decomposition shows that ENSO remains an important source of interannual GMSTA variability, its contribution represents a progressively smaller fraction of the total anomaly as the anthropogenic warming background continues to increase. Such a result is consistent with earlier research showing that ENSO operates on top of a longer-term externally forced warming signal and can substantially modify global surface temperature on interannual timescales (Trenberth et al., 2002; Foster and Rahmstorf, 2011; Lean and Rind, 2008). Furthermore, the changing balance between these two components provides useful context for interpreting exceptionally warm years, particularly when comparing events occurring under substantially different background climate states.

https://doi.org/10.5194/egusphere-2026-5348
Preprint. Discussion started: 7 September 2026

The 2026-2027 event illustrates the opposite side of this relationship. As shown by this study, an exceptionally strong El Niño can still produce a large absolute temperature response, primarily acting as a transient amplification of an already elevated background state, even when the anthropogenic component remains dominant. This interpretation is also relevant with the broader literature on the interaction between ENSO variability and long-term warming, as well as with evidence that the characteristics and impacts of extreme El Niño events may change under continued greenhouse warming (Cai et al., 2014; Cai et al., 2021; Shin et al., 2022).

Retrospective verification also provides some insight into the structure of the ENSO-temperature relationship. The substantial improvement over the simple trend-ENSO formulation suggests that a fixed linear sensitivity does not fully capture how the global temperature response to ENSO evolves across different background climate states. Allowing this sensitivity to change with the warming trend therefore appears to provide useful predictive information, rather than simply adding complexity to the model. At the same time, the benchmark comparison cannot establish that TESR represents the uniquely correct formulation of this relationship. Its main implication is more limited but important: accounting for changes in the background state can improve the representation of interannual temperature variability when ENSO is used as a predictor. That improvement in average predictive performance does not, however, remove the difficulties associated with the upper tail of the distribution.

The sensitivity experiment further highlights the difficulty of estimating the probability of an extreme threshold crossing. A correction of only a few tenths of a degree at the simulated peak changes the March 2027 probability of exceeding +2.0 °C from 23.7 % to 45.19-59.76 % over the empirically observed range of historical peak underestimation. Such a large change in probability for a relatively small adjustment in temperature illustrates how strongly the upper tail of the distribution depends on the model's ability to reproduce the amplitude of exceptional warming events. The effect is much less consequential for the +1.5 °C threshold, which is already reached with very high probability in the central scenario. For the +2.0 °C threshold, however, the central estimate should therefore be interpreted together with its sensitivity range rather than as a precisely constrained probability.

Regarding decision-making, the value of TESR lies primarily in its ability to translate an evolving ENSO scenario into a quantitative estimate of its potential contribution to global temperature extremes. Rather than providing a standalone forecast, such information could help forecasters, risk analysts and public institutions distinguish between the persistent warming background and the temporary amplification associated with an exceptional ENSO event. In practice, repeatedly updating the analysis as ENSO forecasts converge could provide an early indication of how the likelihood of crossing temperature thresholds is changing, while also showing how sensitive that risk remains to uncertainty in the projected peak amplitude. Extending the framework to regional temperatures, additional modes of natural variability and multiple ENSO scenarios would make such information more directly relevant to impact-oriented applications. Once fully observed, the 2026-2027

https://doi.org/10.5194/egusphere-2026-5348
Preprint. Discussion started: 7 September 2026

event will ultimately provide a valuable opportunity to assess whether the relationships identified from the historical record remain applicable under an ENSO amplitude outside the calibration range.

6 Conclusions

The 2026-2027 El Niño represents a significant opportunity to assess to what extent internal climate variability can alter global temperatures by pushing them beyond what would be otherwise explainable with the long-term anthropogenic warming trend alone. Using TESR, we explored how strongly and when the GMSTA could react to a projected record-breaking El Niño for the modern era over the period August 2026 - August 2027, assuming Niño 3.4 as the sole predictor. Our findings show that the El Niño's net contribution to the GMSTA balance could reach about +0.36 °C at its peak, resulting in a maximum median GMSTA of +1.91 °C above pre-industrial levels in March 2027, while the H1 2027 could end as hot as +1.88 °C in the median modelled outcome, with a lower probability of a ≥ +2 °C mean. Year-wise, 2027 is highly likely to be the hottest year since instrumental records began, ranging from +1.57 to +1.92 °C, as the current hottest year recorded is currently held by 2024 with a +1.6 °C corresponding GMSTA. On the other hand, 2026 is likely to range from the 4th to the 2nd hottest year ever recorded in the instrumental record, ranging from +1.44 to +1.59 °C with a median of +1.51 °C. Consequently, the probability of exceeding the first critical threshold of the Paris Agreement (+1.5 °C) is significantly boosted by El Niño, rising from 64 % in a counterfactual ENSO-neutral scenario to 100 % under the factual 2026-2027 ENSO experiment, a 1.6-fold increase, while the probability of sustaining above 1.5 °C remains near 100 % throughout December 2026 - July 2027, indicating a strong ENSO-induced planetary warming during most of late 2026 and first half of 2027. Furthermore, the chance of surpassing +2.0 °C jumps from near zero to 23.7 % in March 2027, a number that could rise to 45.19-59.76 % when accounting for observed peak underestimation.

In addition, our results further demonstrate that while ENSO's relative contribution to overall GMSTA tends to decrease as human-induced global warming intensifies, the absolute ENSO contribution continues to strengthen alongside event intensity, as evidenced by the estimated +0.36 °C peak 2026-2027 contribution, the largest in absolute terms among four analyzed episodes, albeit not the largest relatively (about 19 % of the total versus 30 %, 23 % and 16 % for the 1982-1983, 1997-1998 and 2015-2016 episodes, respectively). An exceptionally strong El Niño can thus provoke a notable short-term spike in global temperatures without being the primary driver of longstanding warming.

TESR's predictive accuracy, validated through retrospective verification, displays a 47.4 % RMSE reduction against a simple trend-ENSO OLS benchmark, while the Diebold-Mariano test confirms statistically significant performance differences, alongside with the probabilistic framework achieving a Brier Skill Score of 0.798 concerning the +1.0 °C threshold. However, the reliability of tail probabilities remains questionable due to the limited number of extreme historical occurrences, and future predictions about ENSO magnitude provide substantial uncertainty despite positive retrospective performance indicators. Future developments of the model could include an extension to regional teleconnections, additional

https://doi.org/10.5194/egusphere-2026-5348
Preprint. Discussion started: 7 September 2026

modes of natural variability, and a wider range of ENSO scenarios in order to better capture the GMSTA response well in advance and to reduce the present-version biases.

Code and data availability

The source code used for data preprocessing, model fitting, lag selection, walk-forward validation, benchmark comparison, probabilistic verification, uncertainty estimation, attribution experiments, and figure generation is available in a public GitHub repository https://github.com/Baptiste-pro/GMSTA-TESR-model, with a versioned archive and DOI provided through Zenodo (https://doi.org/10.5281/zenodo.22287254), including the data files used to run the code and the results of the model in csv format. The version of the code corresponding to the present manuscript is **V1.0.0**.

The analysis combines publicly available observational and reanalysis datasets with a prospective ENSO forecast scenario. The provenance, temporal coverage, retrieval or compilation date, version or dataset identifier, and access information for each external data source are reported below.

1. **Global mean surface temperature anomalies (GMSTA).** The GMSTA time series used as the predictand was obtained from the Copernicus Climate Change Service (C3S) surface air temperature data presented at https://climate.copernicus.eu/surface-air-temperature-july-2026, using the CSV dataset containing all monthly values from the first available graphic on the page. The dataset covers **January 1940 - July 2026** and was retained in YYYY-MM-DD date format. The data were retrieved on **7 August 2026** and subsequently compiled into the model input dataset on **15 August 2026**. The source was last accessed on **15 August 2026**.

2. **Niño 3.4 / ENSO index.** The historical Niño 3.4 index (5°N–5°S, 170°W–120°W) used to construct the ENSO predictor was obtained from ClimateReanalyzer (https://climatereanalyzer.org/research_tools/monthly_tseries/). The underlying ERA5 reanalysis data used in the construction and/or verification of the ENSO series were obtained from the Copernicus Climate Data Store, specifically *ERA5 monthly averaged data on single levels from 1940 to present* (Copernicus Climate Change Service (C3S), 2023; DOI: 10.24381/cds.f17050d7). The historical series used in the model covers **January 1940 to July 2026**. ENSO anomalies were calculated relative to the **1991–2020 climatological baseline**, and the resulting series was retained in **YYYY-MM-DD** format. The data were first retrieved on **7 August 2026** and subsequently compiled on **15 August 2026**. The ERA5 source was last accessed on **15 August 2026**. The smoothing and fixed 3-month ENSO lag specification applied to the ENSO predictor are described in Sect. 3.8.

https://doi.org/10.5194/egusphere-2026-5348
Preprint. Discussion started: 7 September 2026

3. **Prospective 2026-2027 ENSO scenario.** The prospective ENSO forcing was obtained from the ENSO forecast dashboard of The Climate Brink (The Climate Brink ENSO dashboard). The ENSO forecast plume and individual ensemble-member data used in the present analysis were retrieved on **10 August 2026** and subsequently processed for use in the model. The resulting local input files were last modified on **15 August 2026**. The source was last accessed on **15 August 2026**. The prospective simulation was initialized on **1 August 2026**, as described in Sect. 3.4. The central scenario corresponds to a multi-model median peak ONI of +3.96 °C. The exact plume and individual-member data used for the analysis are archived as two CSV files in the study's GitHub repository.

The deposited materials contain the information necessary to reproduce the numerical results reported in this study, including the retrospective forecast origins, the fixed 3-month ENSO lag, benchmark specification, deterministic and probabilistic verification procedures, and the prospective 2026–2027 ENSO scenario used for the reported projections.

Author contributions

Baptiste Boussemart (BB) conceived and designed the study, developed the statistical model and methodology, performed the data analysis, conducted the retrospective and prospective experiments, generated the figures and tables, wrote and revised the manuscript.

Competing interests

BB declares that he has no conflict of interest.

Disclaimer

Copernicus Publications remains neutral with regard to jurisdictional claims made in the text, published maps, institutional affiliations, or any other geographical representation in this paper. While Copernicus Publications makes every effort to include appropriate place names, the final responsibility lies with the authors. Views expressed in the text are those of the authors and do not necessarily reflect the views of the publisher.

Acknowledgements

BB acknowledges the use of GPT-5.6 Luna (https://chatgpt.com) and Claude Sonnet 5 (https://claude.ai). GPT-5.6 Luna assisted to edit the manuscript in order to check the wording and English grammar, as well as to rephrase certain sentences. Claude Sonnet 5 was used for data visualisation and writing the Python code, including the figure production which was

https://doi.org/10.5194/egusphere-2026-5348
Preprint. Discussion started: 7 September 2026

reviewed afterwards. The manuscript was checked in full by BB prior to publication, and all results, conclusions and interpretations are the author's own. BB thanks Météo-Contact (https://meteocontact.fr) for its support in disseminating the results of this study.

Financial support

BB declares that this research received no external financial funding.

References

McPhaden, M. J., Zebiak, S. E., and Glantz, M. H.: ENSO as an integrating concept in Earth science, *Science*, 314, 1740–1745, https://doi.org/10.1126/science.1132588, 2006.

Trenberth, K. E., Caron, J. M., Stepaniak, D. P., and Worley, S.: Evolution of El Niño–Southern Oscillation and global atmospheric surface temperatures, *J. Geophys. Res.*, 107, 4065, https://doi.org/10.1029/2000JD000298, 2002.

Tippett, M. K., & Becker, E. J. Trends, skill, and sources of skill in initialized climate forecasts of global mean temperature. *Geophysical Research Letters*, 51, e2024GL110703. https://doi.org/10.1029/2024GL110703, 2024.

Climate Prediction Center. ENSO: Recent Evolution, Current Status and Predictions. National Oceanic and Atmospheric Administration. https://web.archive.org/web/20260825160051/https://www.cpc.ncep.noaa.gov/products/analysis_monitoring/lanina/enso_evolution-status-fcsts-web.pdf, 2026.

Cai, W., Borlace, S., Lengaigne, M., van Rensch, P., Collins, M., Vecchi, G., Timmermann, A., Santoso, A., McPhaden, M. J., Wu, L., England, M. H., Wang, G., Guilyardi, E., and Jin, F.-F.: Increasing frequency of extreme El Niño events due to greenhouse warming, *Nat. Clim. Change*, 4, 111–116, https://doi.org/10.1038/nclimate2100, 2014.

Cai, W., Santoso, A., Collins, M., et al.: Changing El Niño–Southern Oscillation in a warming climate, *Nat. Rev. Earth Environ.*, 2, 628–644, https://doi.org/10.1038/s43017-021-00199-z, 2021.

Shin, N.-Y., Kug, J.-S., Stuecker, M. F., et al.: More frequent central Pacific El Niño and stronger eastern Pacific El Niño in a warmer climate, *npj Clim. Atmos.* Sci., 5, 101, https://doi.org/10.1038/s41612-022-00324-9, 2022.

Foster, G. and Rahmstorf, S.: Global temperature evolution 1979–2010, *Environ. Res. Lett.*, 6, 044022, https://doi.org/10.1088/1748-9326/6/4/044022, 2011.

https://doi.org/10.5194/egusphere-2026-5348
Preprint. Discussion started: 7 September 2026

Hersbach, H., Bell, B., Berrisford, P., et al.: The ERA5 global reanalysis, *Q. J. R. Meteorol. Soc.*, 146, 1999–2049, https://doi.org/10.1002/qj.3803, 2020.

Malardel, S., Wedi, N., Deconinck, W., et al.: A new grid for the IFS, *ECMWF Newsletter*, 146, 23–28, https://doi.org/10.21957/zwdu9u5i, 2016.

Hoerl, A. E. and Kennard, R. W.: Ridge regression: Biased estimation for nonorthogonal problems, *Technometrics*, 12, 55–67, https://doi.org/10.1080/00401706.1970.10488634, 1970.

Stone, M.: Cross-validatory choice and assessment of statistical predictions, *J. R. Stat. Soc. B*, 36, 111–133, https://doi.org/10.1111/j.2517-6161.1974.tb00994.x, 1974.

Golub, G. H., Heath, M., and Wahba, G.: Generalized cross-validation as a method for choosing a good ridge parameter, *Technometrics*, 21, 215–223, https://doi.org/10.1080/00401706.1979.10489751, 1979.

Künsch, H. R.: The jackknife and the bootstrap for general stationary observations, *Ann. Stat.*, 17, 1217–1241, https://doi.org/10.1214/aos/1176347265, 1989.

Tashman, L. J.: Out-of-sample tests of forecasting accuracy: An analysis and review, *Int. J. Forecast.*, 16, 437–450, https://doi.org/10.1016/S0169-2070(00)00065-0, 2000.

Bergmeir, C., Hyndman, R. J., and Koo, B.: A note on the validity of cross-validation for evaluating autoregressive time series prediction, *Comput. Stat. Data Anal.*, 120, 70–83, https://doi.org/10.1016/j.csda.2017.11.003, 2018.

Diebold, F. X. and Mariano, R. S.: Comparing predictive accuracy, *J. Bus. Econ. Stat.*, 13, 253–263, https://doi.org/10.1080/07350015.1995.10524599, 1995.

Brier, G. W.: Verification of forecasts expressed in terms of probability, *Mon. Wea. Rev.*, 78, 1–3, https://doi.org/10.1175/1520-0493(1950)078<0001:VOFEIT>2.0.CO;2, 1950.

Murphy, A. H.: A new vector partition of the probability score, *J. Appl. Meteorol.*, 12, 595–600, https://doi.org/10.1175/1520-0450(1973)012<0595:ANVPOT>2.0.CO;2, 1973.

Newey, W. K. and West, K. D.: A simple, positive semi-definite, heteroskedasticity and autocorrelation consistent covariance matrix, *Econometrica*, 55, 703–708, https://doi.org/10.2307/1913610, 1987.

https://doi.org/10.5194/egusphere-2026-5348
Preprint. Discussion started: 7 September 2026

Luo, J.-J., Masson, S., Behera, S. K., Shingu, S., and Yamagata, T.: Seasonal Climate Predictability in a Coupled OAGCM Using a Different Approach for Ensemble Forecasts, *J. Climate*, 18, 4474–4497, https://doi.org/10.1175/JCLI3526.1, 2005.

Scott, D. W.: Multivariate density estimation: Theory, practice, and visualization, *Wiley*, https://doi.org/10.1002/9780470316849, 1992.

Lean, J. L. and Rind, D. H.: How natural and anthropogenic influences alter global and regional surface temperatures: 1889 to 2006, *Geophys. Res. Lett.*, 35, L18701, https://doi.org/10.1029/2008GL034864, 2008.

Armstrong McKay, D. I., Staal, A., Abrams, J. F., et al.: Exceeding 1.5 °C global warming could trigger multiple climate tipping points, *Science*, 377, eabn7950, https://doi.org/10.1126/science.abn7950, 2022.